

# Impact of chlorine ion chemistry on ozone loss in the middle atmosphere during very large solar proton events

Monali Borthakur<sup>1</sup>, Miriam Sinnhuber<sup>1</sup>, Alexandra Laeng<sup>1</sup>, Thomas Reddmann<sup>1</sup>, Peter Braesicke<sup>1</sup>, Gabriele Stiller<sup>1</sup>, Thomas von Clarmann<sup>1</sup>, Bernd Funke<sup>2</sup>, Ilya Usoskin<sup>3</sup>, Jan Maik Wissing<sup>4</sup>, and Olesya Yakovchuk<sup>4</sup>

<sup>1</sup>Institute of Meteorology and Climate research, Karlsruhe Institute of Technology, Karlsruhe, Germany

<sup>2</sup>Instituto de Astrofísica de Andalucía, CSIC, Granada, Spain

<sup>3</sup>University of Oulu, Oulu, Finland

<sup>4</sup>University of Rostock, Rostock, Germany

**Correspondence:** Monali Borthakur (monali.borthakur@kit.edu)

## Abstract.

Solar coronal mass ejections can accelerate charged particles, mostly protons, to high energies, causing Solar ~~Partiele~~-Proton Events (SPEs). Such energetic particles can precipitate upon the Earth's atmosphere, mostly in polar regions because of the geomagnetic shielding. Here, SPE induced chlorine activation due to ion-chemistry can occur and the activated chlorine depletes ozone in the polar middle atmosphere. We use ~~a~~-state of the art 1D stacked-box ~~model-called~~-Exoplanetary Terrestrial Ion Chemistry ~~model~~ (ExoTIC), of atmospheric ion and neutral composition to investigate such events in the Northern Hemisphere (NH). ~~Measurement data from the Michelson Interferometer for Passive Atmospheric Sounding (MIPAS) on ENVISAT were used to evaluate the model results using the Halloween SPE~~ The Halloween SPE that occurred in late October 2003, a well-known large event, is used as a test field for our study. This event has been extensively studied before using different 3D models and satellite observations. Our main purpose is to use such a large event that has been recorded by MIPAS on ENVISAT to evaluate the performance of the ion-chemistry model. Sensitivity tests were carried out for different model settings with a focus on the chlorine species of HOCl and ClONO<sub>2</sub> as well as O<sub>3</sub> and reactive nitrogen, NO<sub>y</sub>. The model ~~studies were carried out in the northern hemisphere for simulations were performed in the Northern Hemisphere at~~ a high latitude of 67.5°N, inside the polar cap. Comparison of the simulated effects against MIPAS observations for the Halloween SPE revealed a rather good temporal ~~and spatial agreement~~agreement, also in terms of altitude range for HOCl, ~~ozone~~-O<sub>3</sub> and NO<sub>y</sub>. For ClONO<sub>2</sub>, a good ~~spatial~~spatial agreement was found ~~The in terms of altitude range. The model showed ClONO<sub>2</sub> enhancements after the peak of the event. The~~ best model setting was the one with full ion-chemistry where O(<sup>1</sup>D) was set to photo-chemical equilibrium. HOCl and ozone changes are very well reproduced by the model, specially for ~~night-time~~nighttime. HOCl was found to be the main active chlorine species under ~~night-time~~nighttime conditions resulting in an increase of more than 0.2 ppbv. Further, ClONO<sub>2</sub> enhancements of 0.2-0.3 ppbv have been observed both during daytime and ~~night-time~~. ~~In a nutshell, the most appropriate model setting delivers satisfying result, i.e. the model can be considered to be positively validated.~~nighttime. Model settings that compared best with MIPAS observations were applied to an extreme solar event that occurred in 775 A.D., presumably ~~a~~-once in a 1000 year event. With the model applied to this scenario, assessment can be made what is to

be expected at worst for effects of a SPE on the middle atmosphere concentrating on effects of ion-chemistry compared to  
25 crude parameterisations. Here, a systematic analysis comparing the impact of the Halloween SPE and the extreme event on the  
Earth's middle atmosphere is presented. As seen from the model simulations, both events were able to perturb the polar strato-  
sphere and mesosphere, with a high production of  $\text{NO}_y$  and  $\text{HO}_x$ . Longer lasting and stronger stratospheric ozone loss was  
~~also~~ seen for the extreme event. Qualitative difference between the two events and a long lasting impact on HOCl and HCl for  
the extreme event was found. Chlorine ion-chemistry contributed to a stratospheric ozone loss of 2.4% ~~during for~~ daytime and  
30 10% ~~during night-time during for nighttime during~~ the Halloween SPE as seen with time dependent ionisation rates applied to  
the model. Furthermore, while comparing the ~~two events~~ Halloween SPE and the extreme scenario, with ionisation rate profiles  
applied just for the event day, the inclusion of chlorine ion-chemistry added an ozone loss of 10% and 20% ~~was found during~~  
~~the Halloween SPE and the extreme event respectively~~ which was due to the impact of chlorine ion-chemistry ~~respectively~~.

## 1 Introduction

35 High ~~energetic~~ energy particles (e.g. electrons and protons) that precipitate at high latitudes can alter the chemical compo-  
sition of the atmosphere by different photo-chemical reactions. This mainly happens due to primary collision processes and  
subsequent ion and neutral chemistry reactions. Such reactions ordered by increasing energy are, for example, excitation,  
photo-dissociation, photo-ionisation and dissociative ionisation. These particles can come from various sources in outer space,  
accelerated by different processes to different energies. They affect different altitude ranges of the atmosphere. Such sources  
40 are, for example, galactic cosmic rays (GCRs), with protons and heavier nuclei of energies ranging from hundreds of MeV to  
GeV; coronal mass ejections and ~~solar particle events~~ SPEs with protons of energies from MeV to GeV ~~that precipitate into~~  
~~the earth's atmosphere during solar proton events~~; auroral electrons during substorms accelerated to energies from 10 keV to  
hundreds of keV; and medium and high energy electrons in the radiation belts to energies from tens of keV into the MeV range.  
This ~~mainly happens due to primary collision processes and subsequent ion and neutral chemistry reactions~~. ~~This study involves~~  
45 ~~solar particle events (SPEs)~~ study involves SPEs which can also induce geomagnetic disturbances in the ~~earth~~ Earth's magne-  
tosphere leading to energetic electron precipitation (EEP) events. Recent studies ~~of~~, such as Verronen et al. (2005), that studied  
energetic particle precipitation events (EPP) found significant co-variability in mesospheric ozone. ~~This finding highlighted~~  
~~the need to improve ion chemistry modeling in the D-region for altitudes below 90 km in the ionosphere (Funke et al., 2011)~~  
~~to capture the EPP ozone interaction~~. with proton and electron fluxes.  $\text{HNO}_3$  increases measured during ~~solar proton events~~  
50 ~~(SPE)~~ SPEs cannot be reproduced using the standard parameterization of  $\text{HO}_x$  and  $\text{NO}_x$  production, while models consider-  
ing D-region ion-chemistry in detail agree with the observations (Verronen et al., 2016). This finding highlighted the need to  
improve ion chemistry modeling in the D-region for altitudes below 90 km in the ionosphere (Funke et al., 2011) to capture  
the EPP ozone interaction. The  $\text{HO}_x$  and  $\text{NO}_x$  parameterization cannot reproduce the longer-term effects of ion-chemistry on  
for example, reactive nitrogen partitioning, ozone, and dynamics of the middle atmosphere (Kvissel et al., 2012).

55 In the case of parameterized  $\text{NO}_x$ , NO is produced when  $\text{N}(^2\text{D})$  reacts with molecular oxygen, shown in Reaction ~~R1~~ R1 (Porter et al., 1976; Jackman et al., 2005). This reaction is a major source of NO in the stratosphere, mesosphere and lower thermosphere (Rusch et al., 1981; Barth, 1992).



~~$\text{O}_2$  can also react with the ground state  $\text{N}(^4\text{S})$ , that is temperature dependent and is a major source of NO in the thermosphere above  $\sim 120$  km (Sinnhuber et al., 2012; Barth, 1992) . NO can be destroyed by Reaction R2, which is an effective loss~~  
60 mechanism for  $\text{NO}_x$ , also known as the scavenging reaction (Jackman et al., 2005):



$\text{O}_2$  can also react with the ground state  $\text{N}(^4\text{S})$ , that is temperature dependent and is a major source of NO in the thermosphere above  $\sim 120$  km (Sinnhuber et al., 2012) (Barth, 1992). The excited states of N form NO, while ground state can destroy NO which is relevant in the stratosphere, mesosphere and lower thermosphere. The partitioning between the ground and the excited states determine the amount of  $\text{NO}_x$  formed (Sinnhuber et al., 2012; Nieder et al., 2014) thereby making Reaction R2 the driver  
65 of parameterised  $\text{NO}_x$ . Thus, Reaction R2 makes the difference between full ion-chemistry and parameterised  $\text{NO}_x$  formation. The main processes responsible for the odd hydrogen ( $\text{HO}_x = \text{H}, \text{OH}, \text{HO}_2$ ) formation during energetic particle precipitation events, along with the ion-chemistry processes leading to its release were considered by Solomon et al. (1981). They take place after the initial formation of ion pairs. Solomon et al. (1981) considered the ion-chemistry processes leading to a release of  
70  $\text{HO}_x$  during energetic particle precipitation events. They found that the main process responsible is the uptake of water vapour into large cluster ions and the subsequent release of H during recombination reactions of these cluster ions. Large cluster ions can then be formed by reaction pathways like (Sinnhuber et al., 2012):



These protonised water cluster ions can then recombine with electrons to form H and OH.



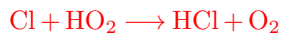
~~During SPEs, highly energetic solar protons and the secondary electrons also ionize neutral species and produce hydrogen and nitrogen radicals leading~~ Hydrogen and nitrogen radicals lead to ozone destruction through catalytic cycles in the strato-  
75 sphere and mesosphere. Different studies found ozone depletion in the mesosphere during SPEs, for example, Weeks et al. (1972) who studied a large polar cap absorption event in 1969 that was explained as a result of the formation of odd hydrogen (Swider and Keneshea, 1973). ~~The chlorine catalytic cycles of ozone destruction are very efficient around 40 km (Lary, 1997). SPE induced changes of chlorine species can contribute to the short-term ozone depletion occurring after the SPE (von Clarmann et al., 2005). This influence is indirect and is mainly caused by  $\text{NO}_x$  and  $\text{HO}_x$  enhancements. The hypochlorous~~

80 ~~acid (HOCl) catalytic cycle acts as a link between chlorine and HO<sub>x</sub> enhancements as a result of the SPEs, which then speeds up the following three reaction sequence involving Reactions R18, R21 and R19:-~~



~~von Clarmann et al. (2005) showed an enhancement of chlorine monoxide, ClO and HOCl immediately after the SPE. They concluded that this was due to the Reactions R21 and R19. During an SPE, HOCl and reactive Cl present in the stratosphere can react with OH and HO<sub>2</sub> respectively, to form ClO. Other reactions of Cl with HO<sub>2</sub> and H<sub>2</sub>O<sub>2</sub> can yield in the production of HCl, which is the most important stratospheric reservoir species of Cl. The Reactions R24, R25, R26 and R27 are relevant to the study in Sect. 4.-~~

85 ~~of HCl, which is the most important stratospheric reservoir species of Cl. The Reactions R24, R25, R26 and R27 are relevant to the study in Sect. 4.-~~



~~SPE induced NO<sub>x</sub> enhancements is essential regarding production of ClONO<sub>2</sub>. López-Puertas et al. (2005) and von Clarmann et al. (2005) reported the first experimental confirmation of Reaction R32 under SPE conditions.-~~



90 ~~During SPEs, NO<sub>x</sub>, HO<sub>x</sub> and chlorine catalytic cycles are responsible for ozone loss in the middle atmosphere at different altitudes.-~~

### 1.1 Hydrogen catalytic cycles

Catalytic cycles involving HO<sub>2</sub> are very important in the lower stratosphere (10-30 km). The fastest of these cycles is shown in Reactions R6, R7 and R8.

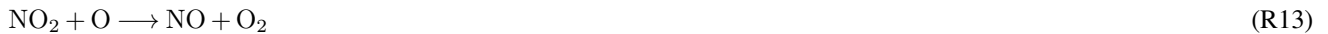


Another example of HO<sub>x</sub> catalytic destruction cycles that is important in the middle and upper mesosphere (above 60 km), is shown in Reactions R9 and R10 (Bates and Nicolet, 1950). In every chain of Reactions R9 and R10, one molecule of O<sub>3</sub>, O(<sup>3</sup>P) or O(<sup>1</sup>D) is lost while reforming H and OH and thereby producing a net ozone loss (Reaction R11).



## 1.2 Nitrogen catalytic cycle

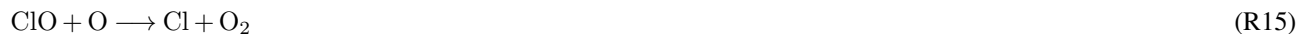
In the lower stratosphere, ozone loss is mainly due to the catalytic cycle with NO<sub>x</sub> governed by the Reactions R12 and R13 in which case the loss of ozone is more persistent due to the longer lifetimes of NO<sub>x</sub>.



## 100 1.3 Chlorine catalytic cycles

The focus of this paper is the impact of charged chlorine species during a SPE. Negative chlorine species constitute a significant part of the total anions in the mesosphere (Chakrabarty and Ganguly, 1989; Fritzenwallner and Kopp, 1998). The chlorine negative ion is [the most important and abundant](#) ion of the lower D region during [day and night](#) [daytime and nighttime](#). Other D region negative ions like O<sub>2</sub><sup>-</sup>, O<sup>-</sup>, CO<sub>3</sub><sup>-</sup>, OH<sup>-</sup>, NO<sub>2</sub><sup>-</sup> and NO<sub>3</sub><sup>-</sup> can react with HCl to produce Cl<sup>-</sup> which forms Cl<sup>-</sup>(X), where X = (HCl, H<sub>2</sub>O, CO<sub>2</sub> and HO<sub>2</sub>) (Kopp and Fritzenwallner, 1997). Cl<sup>-</sup> and Cl<sup>-</sup>(H<sub>2</sub>O) are the most abundant chlorine ions in the mesosphere [as indicated by previous studies for e.g., Chakrabarty and Ganguly \(1989\), Fritzenwallner and Kopp \(1998\) and Turco \(1977\)](#). Both species can react with atomic hydrogen re-releasing HCl and some of the recombination reactions of negative chlorine species with positive ions like H<sup>+</sup> release Cl, ClO, ClNO<sub>2</sub> and Cl<sub>2</sub>. Since the ion reactions are faster, the SPE impacts due to chlorine ion-chemistry are expected to occur without any notable delay. The reactions involving charged and uncharged chlorine species along with the reaction rate coefficients are given in Table A1.

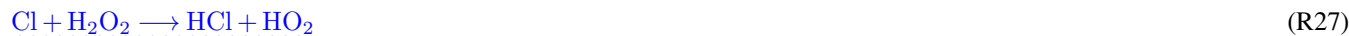
Apart from the NO<sub>x</sub> and HO<sub>x</sub> catalytic cycles, solar proton events can also affect stratospheric chlorine chemistry, but whether solar protons effectively activate or deactivate chlorine depends on illumination conditions. The ion production rates increase during a SPE and influence the chemistry of both charged and uncharged chlorine species. The neutral compounds of chlorine can then contribute to ozone loss. The [chlorine catalytic cycles of ozone destruction are very efficient around 40 km](#) (Lary, 1997). [SPE induced changes of chlorine species can contribute to the short-term ozone depletion occurring after the SPE \(von Clarmann et al., 2005\). This influence is indirect and is mainly caused by NO<sub>x</sub> and HO<sub>x</sub> enhancements. The ClO<sub>x</sub> ozone loss catalytic cycle, where ClO photolyses:](#)



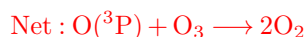
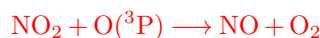
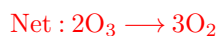
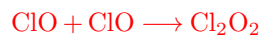
is the main cycle responsible for ozone loss in the middle and upper stratosphere between 40 and 50 km (Daniel et al., 1999). ~~Other uncharged chlorine cycles, for example, ClO<sub>x</sub> cycle where two molecules of chlorine monoxide react with each other~~ (Reactions R26, R27, R28, R29 and R30) is mainly effective between 20 and 30 km (Lary, 1997). O is formed by the photolysis of O<sub>2</sub> and O<sub>3</sub> and is available during daytime. The catalytic cycle involving hypochlorous acid (HOCl) and ClO acts as a link between chlorine and HO<sub>x</sub> enhancements as a result of the SPEs (Reactions R19, R20, R21, R22 and R23) (Lary, 1997). HOCl can photolyse during daytime and the OH formed can react with O<sub>3</sub> reforming HO<sub>2</sub> and Cl reforming ClO thereby recycling HOCl again through Reaction R19. This cycle mainly plays a role in the sunlit polar lower stratosphere (Lary, 1997). Reactive Cl can also be formed via reaction of OH with HCl.



von Clarmann et al. (2005) showed an enhancement of chlorine monoxide, ClO and HOCl immediately after the SPE. They concluded that this was due to the Reactions R21 and R19. During an SPE, HOCl and reactive Cl present in the stratosphere can react with OH and HO<sub>2</sub> respectively, to form ClO. Other reactions of Cl with HO<sub>2</sub> and H<sub>2</sub>O<sub>2</sub> can yield in the production of HCl, which is the most important stratospheric reservoir species of Cl. The Reactions R24, R25, R26 and R27 are relevant to the study in Sect. 4.



This is another effective ozone loss cycle involving SPE induced NO<sub>x</sub> enhancements between 15 and 40 km (Lary, 1997).  
~~As suggested by J. C. Farman and Shanklin (1985), the cycle of chlorine monoxide reacting~~ ClO can react with nitric oxide  
 (Reactions R28, R29, R30 and R31), that is most important in the 15 to 50 km altitude range =



135 ~~However, ClO can also react~~ as suggested by J. C. Farman and Shanklin (1985). NO<sub>x</sub> enhancements are also  
essential regarding the production of ClONO<sub>2</sub>. López-Puertas et al. (2005) and von Clarmann et al. (2005) reported the first  
experimental confirmation of Reaction R32 under SPE conditions. ClO reacts with nitrogen dioxide, NO<sub>2</sub> which is most ef-  
 ficient in the lower stratosphere ~~(Reactions R32, forming ClONO<sub>2</sub> (Reactions R32, R33, R34, R35 and R36),~~ and is another  
effective ozone loss cycle between 15 and 40 km (Lary, 1997).



The present paper deals with changes of HOCl, ClONO<sub>2</sub>, ozone and NO<sub>y</sub> occurring in the Northern Hemisphere at a high latitude of 67.5°N during the Halloween SPE from mid October to early November 2003, peaking around October 28-29. The Halloween SPE was one of the largest SPEs in the satellite era and consisted of a series of solar flares and coronal mass ejections. Such large events mainly occur in the declining phase of the solar maximum. Changes in the composition of HOCl, ClONO<sub>2</sub>, ozone and NO<sub>y</sub> species during the Halloween SPE have been previously reported in Funke et al. (2011) and Jackman et al. (2008). Funke et al. (2011) used different models to investigate the SPE induced changes and Jackman et al. (2008) used version 3 of the Whole Atmosphere Community Climate Model (WACCM). Both studies compared with the MIPAS observations from polar orbit satellite ENVISAT. Damiani et al. (2012) also looked at chlorine species (i.e., HOCl, ClONO<sub>2</sub>, ClO and HCl) using MLS and MIPAS data and version 4 of the WACCM model during SPEs of 17 and 20 January 2005. However they did not consider the D region ion-chemistry. Here, we studied the temporal evolution of changes of the respective chemical constituents considering the D region ion-chemistry in ~~a the~~ 1D stacked box model, Exoplanetary Terrestrial Ion Chemistry (ExoTIC). The ion-chemistry was implemented by Winkler et al. (2009) upon which ExoTIC is based, ~~but we compare with the MIPAS observations, which provide a better picture of the polar cap region compared to Winkler et al. (2009) who compared HALOE HCl observations that were less densely sampled than MIPAS data.~~

In order to have a better comparison of ExoTIC simulations with MIPAS observations, we ensured that they are sampled inside the polar vortex. The polar vortex is a large circumpolar cyclone ~~which dominates the circulation that is formed due to decreased solar insolation~~ in the polar winter stratosphere ~~which forms due to decreased solar insolation as a manifestation of a strong meridional temperature gradient caused by a lack of high-latitude solar heating during polar night and dominates the dynamics~~ (Harvey et al., 2015). The assumption is that the air inside the polar vortex is horizontally well mixed and separated from air masses outside the vortex. That allows us to simulate it in a 1D vertical model. The ionisation during particle precipitation in the polar cap is also assumed to be inside the polar vortex where NO<sub>x</sub> is conserved which makes it better comparable to the 1D model. The procedure is described in detail in the Sect. 3.1.

The Halloween SPE is later compared with an exceptionally strong cosmic ray event that occurred in ~~774/775~~ A.D. It was derived from the historical records in radiocarbon <sup>14</sup>C measured in tree ring archives and later confirmed by <sup>10</sup>Be and <sup>36</sup>Cl cosmogenic nuclides. Although various scenarios were initially proposed, it is concluded now that the event was caused by solar energetic particles (Sukhodolov et al., 2017). <sup>10</sup>Be and <sup>14</sup>C implied that the event had a very hard spectrum and thereby very high energetic protons. It is the ~~greatest strongest~~ solar energetic particle storm known for the last 11 millennia (the Holocene), serving as a likely worst-case scenario being 40–50 times stronger than the largest directly observed event on 23<sup>rd</sup> February 1956 (Usoskin et al., 2013). This event was transient, as estimated using the ratio of different cosmogenic isotopes (Mekhaldi et al., 2015).

This paper is organised as follows. ~~Section Sect.~~ 2 describes the ionisation rates, model framework, simulations and the satellite observations used to evaluate the model. ~~Section Sect.~~ 3 presents the results of the model evaluation with MIPAS satellite observations. An overview of the changes in chlorine species, ozone and NO<sub>y</sub> induced by the SPE is presented. ~~Section Sect.~~ 4 presents a case study comparing model simulations of the Halloween SPE with the extreme solar event. ~~Section Sect.~~ 5 shows some results describing the impact of chlorine ion-chemistry on ozone loss. In sect. 6, a conclusion is provided



to check if the data is well understood, a summary of how our results compare to previous studies. Finally an assessment is  
175 given how further studies could improve our current knowledge on SPE induced ozone loss due to chlorine ion-chemistry.

## 2 Data and methods

### 2.1 Ionisation rates

The ionisation rates (IRs) used for the Halloween SPE were obtained from the Atmospheric Ionisation during Substorm (AIS-storm) model which is an enhanced version of the Atmospheric Ionisation Module Osnabrück (AIMOS) model (Wissing and  
180 Kallenrode, 2009). The AIMOS model computes ~~ionization~~ ionisation rates by precipitating electrons, protons and alpha particles for the whole atmosphere based on particle flux measurements from Polar Operational Environmental Satellites (POES), the Meteorological Operational satellites (Metop) and the Geostationary Operational Environmental Satellites (GOES). The treatment of the electron fluxes is in the energy range (0.154–300 keV), protons ~~have with~~ an energy range of 0.154 eV to 500 MeV. In the AIMOS v2.0-AISstorm model, both the time resolution (0.5 hr) and spatial resolution has been improved  
185 compared to AIMOS. For a comparison of the model results with MIPAS observations, the time dependent ionisation rates were put into ExoTIC. Figure 1 on the left side shows the temporal evolution of ion pair production rates for protons, electrons and alpha particles varying over the time period, 25<sup>th</sup> October to 4<sup>th</sup> November 2003 from the AISstorm model. These IRs are averaged over the longitudes for the latitude of 67.5°N, in the polar cap region and are also daily averaged. For the extreme event, integrated ionisation rates were taken from an extreme SPE of 23 February 1956 (SPE 56) (Meyer et al., 1956), which  
190 was the strongest observed event with ground-level enhancement (GLE) > 4000 %. ~~These integrated IRs were scaled by a factor of Cliver et al. (2022) estimated this factor 70 (Usoskin and Kovaltsov, 2012) in order to represent a one in a 1000 year event. The factor 70 × particle fluence compared to the 1956 event and the ionisation rates were scaled accordingly. This factor~~ was a rough estimate to scale the fluxes of particles and excess radiation such that the energy spectrum of SPE 56 was comparable to the isotope signals of the extreme event. Figure 1 on the right shows the ionisation rate profiles for both the  
195 events. The profiles for the Halloween SPE show average IRs for October 27 (day 301) and October 28 (day 302) before the SPE (in blue) and the average IRs for October 28 and October 29 during the main SPE phase (in green). It can be observed that the ionisation rates for the stratosphere and lower mesosphere in case of the extreme event is about 1-2 orders of magnitude higher compared to the Halloween SPE main phase. This is because the extreme event contained protons of energies up to a few GeV, compared to about only a few MeV protons for the Halloween SPE, the ionisation rates for the same can be seen to  
200 reach much further down to the surface.

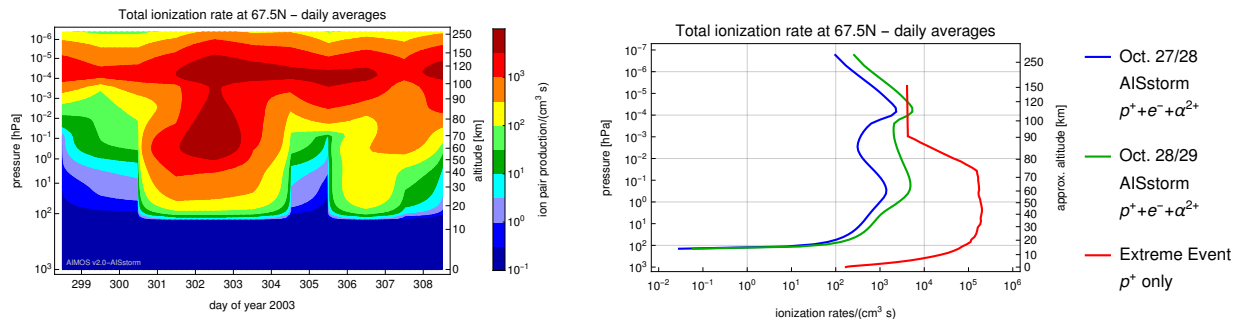


**Figure 1.** Time dependent and daily averaged ionisation rates (IRs) from 25<sup>th</sup> October to 4<sup>th</sup> November 2003 obtained from the AISstorm model for the latitude of 67.5°N (left); Mean ionisation rates (IRs) before the SPE (Oct 27-28), and in SPE main phase (Oct 28-29) obtained from AISstorm and mean IRs of the extreme event for the same latitude of 67.5°N (right).

## 2.2 Description of the 1D model and Experiments

The Exoplanetary Terrestrial Ion Chemistry model ExoTIC is a 1-dimensional stacked-box model of the atmospheric neutral and ion composition (Herbst et al., 2022). The ion-chemistry is based on the UBIC (University of Bremen ion-chemistry) model developed by Winkler et al. (2009) for the terrestrial middle atmosphere. The neutral chemistry is based on the SLIM-CAT model by Chipperfield (1999). It accounts for photo-ionisation of NO by Lyman- $\alpha$  radiation, photo-dissociation of charged species and photo-detachment of electrons but doesn't contain any diffusion or horizontal and vertical transport. It first simulates a neutral atmosphere and contains the time evolution of 106 charged and 58 neutral species, which that interact due to neutral, neutral-ion, and ion-ion gas-phase reactions, as well as photolysis and photoelectron-photo-electron attachment and detachment reactions (Sinnhuber et al., 2012). The model ExoTIC model extends the applicability of UBIC to atmospheres of (rocky) planets other than Earth with a wide range of orbital parameters, stellar systems and base compositions as discussed by Herbst, Konstantin et al. (2019). More neutral species have been added to the ion-chemistry in ExoTIC since studies by Winkler et al. (2009). The ionisation of CO<sub>2</sub> was recently included. Another small change is that the equilibrium is calculated for the ions, which stabilised the model. The model contains boxes of 2.7 km each in height, which is the same as the background atmosphere that is used as input. For the studies performed here, the background atmosphere was taken from the EMAC (ECHAM/MESSy) atmospheric chemistry climate model with T42 horizontal truncation. It has 74 levels in the vertical direction and covers an altitude up to 220 km 200-220 km, depending on latitude and season, with a vertical resolution of 2.7 km. The neutral chemistry and the ion-chemistry model are calculated iteratively as follows:

1. The neutral model is time dependent and calculates the volume mixing ratios of the neutral species with a variable time step and feeds them to the ion-chemistry model.
2. The ion-chemistry in the equilibrium state is calculated, calling it hourly from the neutral model. The highest level for which the ion-chemistry is calculated is 1 (207.4 km) and the lowest level is 53 (25.4 km), which depends on the initialisation.

- 225 3. The net effective production or loss rates of neutral species due to primary ~~ionization~~ionisation, positive and negative ion-chemistry which can also be used as a parameterisation for global chemistry-climate models (Nieder et al., 2014), are computed using an iterative chemical equilibrium approach.
4. The production rates resulting from the ion-chemistry computation are then fed back to the 1-D neutral chemistry model, which solves for the neutral atmospheric state transiently using the net effective production/loss reactions as well as neutral photo-chemistry reactions.
5. Lastly, this state is again returned to the ion-chemistry model for the following computation.

230 The model settings used for the sensitivity studies were mainly variations of full ion-chemistry containing both positive and negative ions from the D-region: setting reactive  $O(^1D)$  in photo-chemical equilibrium and switching off the chlorine ion-chemistry. Parameterised  $NO_x$  and  $HO_x$  model simulations based on Porter et al. (1976) and Solomon et al. (1981) were also carried out to assess the performance of the ~~full~~ ion-chemistry model.

### 2.2.1 ~~Full-Ion-chemistry~~Ion-chemistry

235 The ionisation in this case is driven by prescribed ionisation rates and by photo-ionisation of  $NO$ , with the primary positive charges being distributed onto  $N_2$ ,  $N$ ,  $O_2$  and  $O$  and balanced with electrons (Sinnhuber et al., 2012). ~~The ionisation of  $CO_2$  was recently included.~~ These rates of the primary ions are calculated by ionisation cross-sections based on Rusch et al. (1981) and Jones and Rees (1973). All of the processes like dissociation and dissociative ionisation of  $O_2$  and  $N_2$  as well as ionisation of  $O_2$ ,  $N_2$  and  $O$  can form the excited states of  $N$ ,  $O$ ,  $N_2^+$ ,  $N^+$ ,  $NO^+$  which are also included in the model. More details with a

240 full list of the reactions, reactions rates and references for the reactions rates used for the positive ion-chemistry can be found in Sinnhuber et al. (2012) and the newer versions in Herbst et al. (2022).

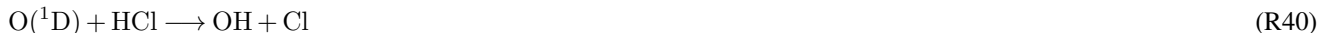
#### ~~Full-ion-chemistry with $O(^1D)$ in photo-chemical equilibrium~~

~~The simulation results are sensitive to the changes of the  $O(^1D)$  is-branching ratio,  $\beta = \Delta O(^1D)/(\Delta O(^1D) + \Delta O(^3P))$  which is discussed in Winkler et al. (2009). Winkler et al. (2011) has reported the  $O(^1D)$  corrections in the UBIC model in~~

245 ~~more detail.  $O(^1D)$  is~~ a reactive species which is formed from the dissociation of  $O_2$  and  $CO_2$  by particle impact ionisation but also in the ion-chemistry reactions itself. It generally goes into photo-chemical equilibrium but that is not considered in the ion-chemistry part of the model, so the rate of  $O(^1D)$  formation passed to the neutral chemistry is too large. There are a few other short lived neutral species in the ion-chemistry model, like the excited states of ~~N that are also,~~ ~~for example,  $N(^2D)$ , that are~~ treated like ions. ~~Basically  $O(^1D)$  is produced through the Reaction R1.~~ Since  $O(^1D)$  is short lived mostly but not

250 considered to go into equilibrium in the ion-chemistry stage, a large rate of formation of  $O(^1D)$  is produced and added to the neutral chemistry. ~~The time constants for the quenching  $O(^1D) + M \rightarrow O(^3P) + M$  in the stratosphere are significantly smaller than the chosen integration time step in the ion-chemistry model which was also reported in Winkler et al. (2011). That causes too high  $O(^1D)$  concentrations and an unrealistically strong effect through reaction R37.  $O(^1D)$  can react with species like  $H_2O$ ,  $H_2$  and  $CH_4$  in the lower stratosphere and also with  $HCl$  in the stratosphere to produce  $OH$ . Therefore, setting either the~~

255 formation rates of O(<sup>1</sup>D) to zero or calculating it in photo-chemical equilibrium ~~significantly makes~~ can make a difference to the full ion-chemistry through ~~reactions~~ Reactions R37, R38, R39 and R40.



### 2.2.2 Sensitivity tests switching off the chlorine ion-chemistry

The purpose of this sensitivity test is to study the impact of the chlorine ion, ~~an important negative ion in the lower D region.~~ ~~We also.~~ We wanted to study what difference it makes to the full ion-chemistry with a focus on the ozone loss. This is done  
260 by switching off the reactions of negative chlorine ions with neutrals or the recombination reactions with H<sup>+</sup> in ExoTIC. The relevant reactions are given in Table A1.

### 2.2.3 Parameterised NO<sub>x</sub> and HO<sub>x</sub>

The assumption in case of parameterised NO<sub>x</sub> is that 1.25 N atoms are produced per ion pair when electrically charged particles collide and dissociate N<sub>2</sub>. This process produces N<sub>2</sub><sup>+</sup> and NO<sup>+</sup> ions and, finally, atomic nitrogen. The latter is produced in its  
265 ground state N(<sup>4</sup>S) (45 % or 0.55 per ion pair) and the excited state N(<sup>2</sup>D) (55 % or 0.7 per ion pair). These values are mostly used in stratospheric and mesospheric models. In case of HO<sub>x</sub>, each ion pair typically results in the production of around two HO<sub>x</sub> constituents, i.e. a pair of H and OH per ion pair during recombination of the protonised water cluster ions in the upper stratosphere and lower mesosphere (Reaction R5) which was first estimated by Swider and Keneshea (1973).  
Andersson et al. (2016) calculated the parameterised HO<sub>x</sub> production using a fixed H<sub>2</sub>O profile. In contrast, ExoTIC assumes  
270 a zero abundance of water vapour above 80 km, while below, water vapour is modelled as a pair of H and OH. The HO<sub>x</sub> formation stops when there is no more water vapour. For high water vapour, two HO<sub>x</sub> per ion pair are formed, but the rate decreases with decreasing H<sub>2</sub>O. As the H<sub>2</sub>O profile used in Andersson et al. (2016) decreases strongly above 80 km, the rate of HO<sub>x</sub> production also goes to zero above 80 km. Jackman et al. (2005) also considered this and an ion pair is computed to produce less than two HO<sub>x</sub> constituents per ion pair in the middle and upper mesosphere. In ExoTIC, 2 HO<sub>x</sub> are produced per  
275 ion pair everywhere, but the production of HO<sub>x</sub> is balanced by loss of water vapour, and the production therefore stops when all water vapour is consumed, effectively also reducing the amount of HO<sub>x</sub> production in regions of low water vapor. We choose 2 HO<sub>x</sub> per ion pair because we want to mainly concentrate on middle mesosphere to stratosphere and not upper mesosphere, i.e. above 80 km.

### 2.3 MIPAS on ENVISAT

280 The Michelson Interferometer for Passive Atmospheric Sounding (MIPAS) was a Fourier transform spectrometer for the detection of mid-infrared limb emission spectra in the middle and upper atmosphere on the ~~Envisat~~ ENVISAT (Environmental

Satellite, 2000) mission (Fischer et al., 2008). ENVISAT was launched in 2002 into a sun-synchronous polar orbit (800 km) and stopped operation in April 2012. The atmospheric spectra were inverted into vertical profiles of atmospheric pressure, temperature and volume mixing ratios (vmrs) of more than 30 trace constituents. MIPAS observed a spectral range of 4.15  $\mu\text{m}$  to 14.6  $\mu\text{m}$  with a high spectral resolution, where a wide variety of trace gases have absorption lines and signals that are generally higher than in other parts of the spectrum. This is because the Planck function maximises at about 10  $\mu\text{m}$  for atmospheric temperatures. The measurement strategy of the MIPAS instrument was based on trace gases having characteristic emission and absorption lines, represented by their absorption coefficients, which are unambiguous “fingerprints” of the particular trace gases. The MIPAS mission is separated into two phases, caused by a malfunction of the instrument around March 2004. The first phase of the mission (2002–2004) is usually referred to as the MIPAS full-resolution (FR) period. After the malfunction, operation was resumed with a reduced optical path difference, resulting in deteriorated spectral resolution. The second phase starting in January 2005 is called the reduced-resolution (RR) period. Because of the long optical path through the atmospheric layers, MIPAS could also detect trace gases with very low mixing ratios. Vertical information was gained by scanning the atmosphere at different elevation angles with different tangent altitudes. MIPAS could observe atmospheric parameters in the altitude range from 5 to 68 km nominally with minimum and maximum vertical steps of 1 and 8 km respectively. The MIPAS data are used here for evaluation of the model results with different parameterisations. Data presented here are IMK version V5 data for HOCl, ozone, ClONO<sub>2</sub> and NO<sub>y</sub> species (NO, NO<sub>2</sub>, HNO<sub>3</sub>, N<sub>2</sub>O<sub>5</sub>) that are updates of those published by von Clarmann et al. (2006), von Clarmann et al. (2012), Glatthor et al. (2006), Höpfner et al. (2007a) and Funke et al. (2005).

### 2.3.1 Averaging Kernels

Different vertical resolutions of the MIPAS observations and the model need to be accounted for a meaningful comparison. The ExoTIC model has a vertical resolution of 2.7 km whereas MIPAS has different vertical resolutions for different species. For example, in case of HOCl, the maximum vertical resolution can be 17 km and for ClONO<sub>2</sub>, it can be 13 km at an altitude of 40 km and above as seen from an example Figure 2 for a specific time point.

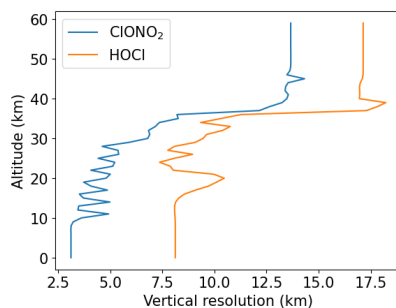


**Figure 2.** Example of typical profiles for the vertical resolution of HOCl and ClONO<sub>2</sub>

To remove the discrepancy of different vertical resolutions between the model and MIPAS observations, the original model profiles have to be convolved and adjusted to the MIPAS altitude resolution. This adjustment procedure yields new species

profiles that MIPAS would see if it were to sound the model atmosphere. For this purpose, we make use of the averaging kernels (Rodgers, 2000) and use a scheme suggested by Connor et al. (1994) to adjust the better resolved model profiles to those of MIPAS and the new adjusted model profiles  $x_{\text{new}}$  are calculated as:

$$x_{\text{new}} = \mathbf{A}x_{\text{orig}} + (\mathbf{I} - \mathbf{A})x_{\text{a}} \quad (1)$$

310 where  $\mathbf{A}$  is the MIPAS averaging kernel matrix,  $x_{\text{orig}}$  is the original model profile,  $\mathbf{I}$  is a unity matrix and  $x_{\text{a}}$  is the a priori information used in the MIPAS retrievals. The rows of the [AK-averaging kernel](#) matrix give the contribution of the true values to the retrieved values and the columns give the response of the delta peak like perturbations at each altitude. Figure 3 shows an example of averaging kernels for the different species and for a profile retrieved from spectra measured at latitude of 67.5°N on  
 315 altitudes. For example, the maximum sensitivity is seen at 20 km for HOCl in this specific case, whereas for ClONO<sub>2</sub>, it is around 15 km. To characterize the vertical resolution, the typical measures are either the full width at half maximum of the rows of the  $\mathbf{A}$  or the gridwidth divided by the respective diagonal of  $\mathbf{A}$  (Rodgers, 2000).

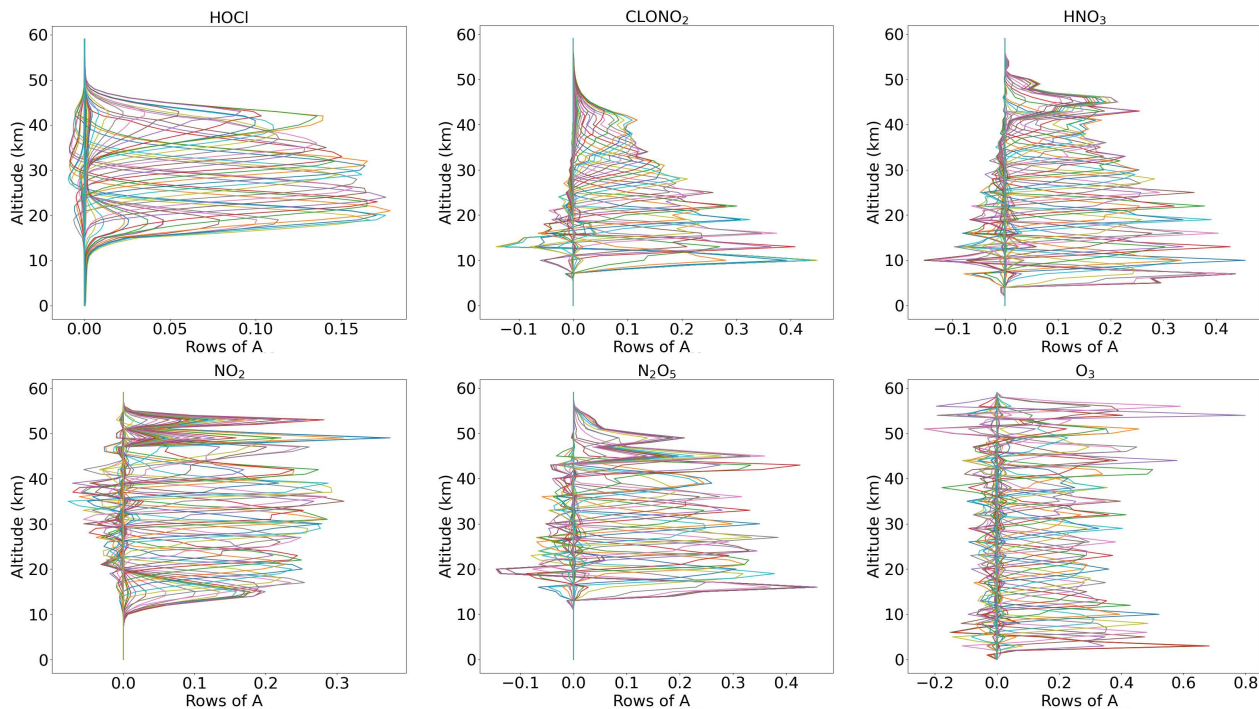


**Figure 3.** Example of rows of Averaging Kernels ( $\mathbf{A}$ ) for typical MIPAS HOCl, ClONO<sub>2</sub>, HNO<sub>3</sub>, NO<sub>2</sub>, N<sub>2</sub>O<sub>5</sub> and O<sub>3</sub> at a latitude of 67.5°N on 27 October 2003 at 00:00 UT.

### 3 Comparison of ExoTIC simulations to MIPAS observations for the Halloween SPE 2003

In this section, a comparison study between the ExoTIC model results and MIPAS observations has been carried out for the chlorine species of HOCl, ClONO<sub>2</sub>, ozone and odd oxides of nitrogen (NO<sub>y</sub>) for the Halloween SPE 2003. The comparison is done for the model simulations with different settings of ion-chemistry, i.e. calculating the photo-chemical equilibrium of O(<sup>1</sup>D) and switching off the uptake of chlorine ions, and parameterised NO<sub>x</sub> and HO<sub>x</sub>. The model simulations are performed for a high latitude of 67.5°N and the MIPAS data were taken for the polar cap region, averaged over geographic latitudes such that it's inside the vortex, either vortex core or vortex edge depending on the tracer properties. The model data is sampled in the MIPAS altitude grid as well. The day and night for the MIPAS data are sorted according to the solar zenith angle (day ≤ 90°; night > 98°). The solar zenith angles for the 1D model were chosen such that, for each day, it is the mean solar zenith angle for the MIPAS data plus/minus the standard error of mean (SEM) with N being the number of data points for each day.

$$\text{SEM} = \frac{\text{Standard Deviation}}{\sqrt{N}} \quad (2)$$

Since ExoTIC doesn't have diffusion or horizontal and vertical transport, the comparison can only be done for a short period of time. The model results are compared with the MIPAS observations for a total of 9 days from 26<sup>th</sup> October to 3<sup>rd</sup> November 2003. Due to different vertical resolutions between the model and MIPAS observations, averaging kernels were applied. [The averaging kernels were applied after sampling the model data in the MIPAS altitude grid.](#) Now, ExoTIC being a 1D column model doesn't produce the output at the same geolocations as MIPAS hence the application of the MIPAS averaging kernels was based on the temperature criteria. The following procedure was applied for the convolution:

1. The model ~~profile from the time series was fixed first~~ [profiles were selected, one at a time, from the entire time series.](#)
2. All the profiles from MIPAS within 57.5 and 77.5 degrees N latitude and +/- 6 hours of the model profile's time were selected.
3. For this obtained MIPAS sample of temperature profiles, the root mean square value was calculated with the model's temperature profile which is fixed for the entire time series.
4. The geolocation for which the root mean square value of the temperature difference profile was minimal was selected, and averaging kernels for this geolocation were applied to the trace gas profiles from the model.

Using this procedure, we have obtained model profiles that were adjusted to the vertical resolution of MIPAS. The data was then averaged daily and the absolute or relative differences w.r.t a day before the event, i.e. 26<sup>th</sup> October 2003 (day 299), was calculated.

#### 3.1 Estimation of the polar vortex edge

There are different methods of estimating the vortex edge and one of the methods widely used is using CO as a tracer of vortex air. Due to its strong vertical gradient and longevity in the polar winter vortex, carbon monoxide is commonly used as a

tracer of vortex air originating from the upper mesosphere and lower thermosphere, ~~which is transported down into the lower mesosphere and stratosphere in the polar vortex.~~ Hence it can be used to estimate the vortex edge. Funke et al. (2005) also used the CO gradient for the vortex boundary definition, which is less dependent on the actual conditions, and also in their case the maximum derivative was around 0.5 ppmv. Here, we have used a CO vmr threshold (discriminating mesospheric air from the background) as vortex criterion. We need an altitude-independent criterion (as we need to differentiate entire profiles) and our short time period (a few days) allows for a time-independent definition. A chemical vortex definition (via CO) is also widely used in the mesosphere (Harvey et al., 2015). And for the chemical species and the SPE responses discussed here, the relevant altitude range is more in the stratosphere. In the stratosphere, the vortex might be considerably smaller and is commonly determined from the potential vorticity. Here, we use the tracer gradient instead to be consistent with the MIPAS observations that we use for comparison. Figure 4 shows volume mixing ratios of CO versus latitude in the Northern Hemisphere for different longitude bins of size 20 (shown by different colours) and averaged over latitude bins of size 5 from 27<sup>th</sup> October (day 300) to 3<sup>rd</sup> November (day 307) ~~November~~-2003 separated by day-time and ~~night-time~~nighttime. Choosing a threshold of 0.5 ppm of CO, the ~~edge of the polar vortex~~ polar vortex boundary can be determined from the corresponding x-axis where an increase of the volume mixing ratios start to occur. An increase is observed starting at a latitude of approximately around 55°N for the different days. The estimation of the polar vortex edge boundary helps to choose the MIPAS sampling of the zonal averages for a better inter-comparison. One can also check the vortex boundary by looking at CH<sub>4</sub> zonal means, for example, Figure 9 of Funke et al. (2011). From that figure and as also discussed in Funke et al. (2011), the boundary is around 60°N which also works well for the stratosphere. We chose the latitude 57°N as to where the vortex begins and defined the latitude bands 57-77°N as "the edge region of the vortex" and the high latitude bands 70-90°N as "deep in the vortex".



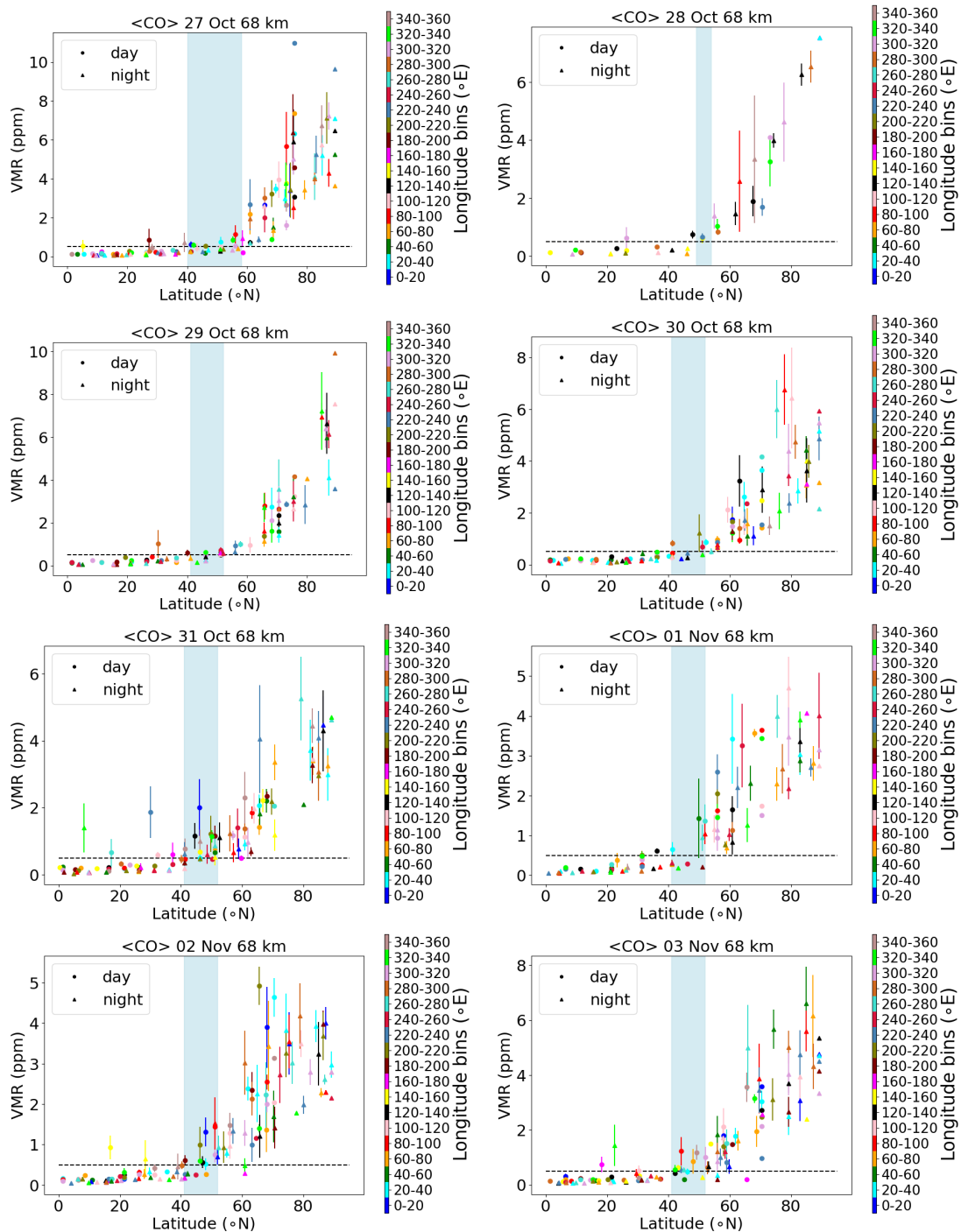


**Figure 4.** MIPAS [daily averaged](#) CO (ppm) as a function of latitude (°N) for longitude bins of size 20 and averaged over latitude bins of size 5 for 27<sup>th</sup> October-3<sup>rd</sup> November 2003 (day and night) at 68 km altitude. Colors mark the longitude bins from 0-20°E to 340-360°E running from blue to rosybrown. The error bars mark the standard error of mean. The light-blue shaded region marks the latitude range of the vortex edge and the dashed horizontal line is the CO threshold of 0.5 ppm.

## 3.2 HOCl change

A comparison of Envisat MIPAS V5 ~~HOCl measurements~~ HOCl measurements (von Clarmann et al., 2006) for the polar Northern Hemisphere (57-77°N) and ExoTIC computations with different settings of HOCl simulation is presented in Figure 5-figures 5 and 6 for daytime and night-time nighttime respectively. The model ~~and the MIPAS data are sampled on the MIPAS altitude grid and the model data~~ is read out in the solar zenith angle range of MIPAS daytime and night-time nighttime observations. The values in Figure 5 both figures 5 and 6 start on the 26<sup>th</sup> October 2003 (day 299). MIPAS observations for HOCl showed significant enhancements with peak values of 0.2 ppb for daytime and 0.24 ppb for night-time nighttime on the 29<sup>th</sup> of October. The model results with ~~full ion-chemistry significantly~~ full ion-chemistry also overestimated the observed enhancements for night-time nighttime by a factor of 4 (around 1.25 ppb), and for day-time by a factor of 3 (around 0.65 ppb) produced at an altitude of 35-40 km. HOCl enhancements below 30 km was also observed for both daytime and night-time nighttime with full ion-chemistry and a peak producing 0.12 ppb was observed in the mesosphere during night-time nighttime. Sensitivity studies were performed setting O(<sup>1</sup>D) to photo-chemical equilibrium that showed a decrease in the enhancements from 1.25 ppb to 0.55 ppb during night-time nighttime and 0.65 ppb to 0.08 ppb during daytime produced by the model also at 35-40 km during the event. The higher mixing ratios of HOCl below 30 km for both daytime and night-time nighttime also disappeared with this setting. Switching off the chlorine ion-chemistry led to the removal of ~~the peak of~~ 0.2 ppb HOCl observed in the mesosphere during night-time nighttime. And similar behaviour was also observed for the parameterised NO<sub>x</sub> and HO<sub>x</sub> model. However, ~~significantly low~~ much lower values were observed during daytime for the model, setting O(<sup>1</sup>D) to photo-chemical equilibrium, without chlorine ion-chemistry and parameterised NO<sub>x</sub> and HO<sub>x</sub> compared to MIPAS observations. Reaction rate constants and photo-chemical data follow in general the JPL-2006 recommendations from Sander et al. (2006).

After the application of averaging kernels the higher mixing ratios produced by the model were ~~significantly~~ smeared out over altitudes and reduced in their peak value. For daytime, the peak value of the full ion-chemistry model decreased from 0.65 ppb to 0.4 ppb. And for the sensitivity studies with O(<sup>1</sup>D) in photo-chemical equilibrium, without chlorine ion-chemistry and parameterised NO<sub>x</sub> and HO<sub>x</sub>, the peak value of 0.08 ppb decreased to 0.03 ppb. ~~For night-time~~ This peak value occurs due to the increased availability of chlorine atoms due to the catalytic ozone destruction cycle. The HOCl concentration reaches a peak around 35 km during daytime because this altitude represents the optimal conditions for the ClO-HOCl catalytic cycle (Reactions R20, R21, R22 and R19) to occur. For nighttime, full ion-chemistry peak value of 1.25 ppb went down to 0.84 ppb after applying the MIPAS averaging kernels. Setting O(<sup>1</sup>D) to photo-chemical equilibrium decreased the peak value from 0.55 ppb to 0.36 ppb which is in better agreement with the MIPAS observations. For the model without chlorine ion-chemistry and parameterised NO<sub>x</sub> and HO<sub>x</sub>, the enhancements of 0.58 ppb went down to 0.33 ppb ~~which that~~ also agrees quite well. Jackman et al. (2008) ~~also~~ compared results from the Whole Atmosphere Community Climate Model (WACCM3) with MIPAS observations and applied MIPAS averaging kernels for the Halloween SPE ~~2003. They 2003 and~~ found the HOCl peak at an altitude of 48 km on the 29<sup>th</sup> of October and the MIPAS averaging kernels moved it down to 40 km. ExoTIC however produced the peak around 35-40 km itself for both daytime and night-time nighttime for all the test cases. This is actually quite in agreement with the MIPAS observations and the application of the averaging kernels also didn't shift the peak in

terms of altitude. This difference in the peak altitude between the results from Jackman et al. (2008) and ExoTIC might be due to the fact that WACCM3 has fully interactive dynamics, radiation, chemistry and other parameterizations whereas ExoTIC includes only the chemistry. Damiani et al. (2012) considered the SPE of January 2005 where they observed 0.2 ppb increase of HOCl during the event in the polar cap region also using the WACCM model that agreed quite well with Microwave Limb  
 405 Sounder (MLS) observations. Enhancements of HOCl results from enhanced HO<sub>x</sub> constituents. In the middle stratosphere, it is mainly accelerated by odd hydrogen chemistry (via Reaction R19). The morphology of the HOCl distribution and its temporal variation is a combined effect of photolysis, temperature and availability of ClO, HO<sub>2</sub> and OH, which in themselves show pronounced diurnal variation.

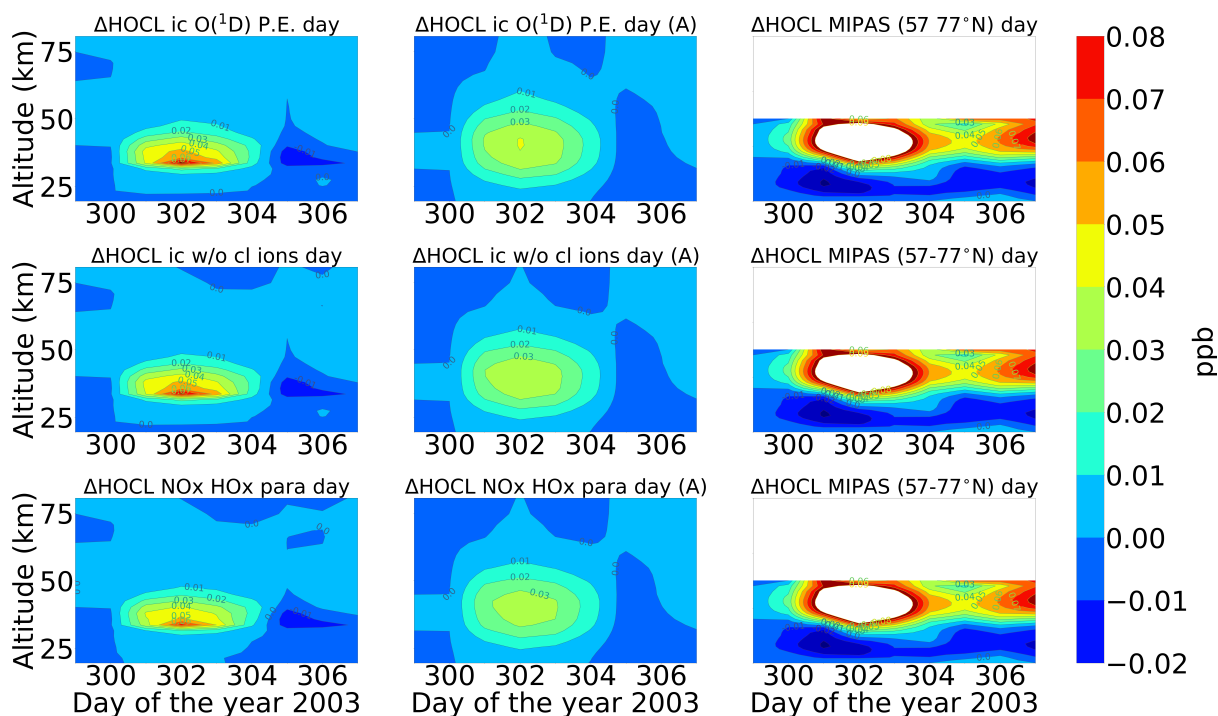


**Figure 5.** Absolute differences of daily averaged data for HOCl w.r.t. a day before the event, i.e. 26<sup>th</sup> October 2003. Starting point is 26<sup>th</sup> October 2003 and for the ~~four~~three different model settings (Sensitivity tests (row-wise): ion-chemistry with O(<sup>1</sup>D) in photo-chemical equilibrium, switching off chlorine ion-chemistry and parameterised NO<sub>x</sub> and HO<sub>x</sub>); column-wise: without Averaging kernel (A), with Averaging kernel (A) applied and MIPAS observations averaged over 57-77°N for day-time (sza ≤ 90°). For daytime, the white region below 50 km is the MIPAS peak (0.2 ppb) and the colorbar is adjusted to the lower mixing ratios predicted by the model (first plot). The white region above 50 km for the MIPAS observations represent meaningless data, where the values of Averaging kernel (A) diagonal elements are close to zero (< 0.03) that indicate no ~~significant~~ sensitivity to the retrieved parameter at the corresponding altitude. Colorbar interval: (-0.02, -0.01, 0.00, 0.01, 0.02, 0.03, 0.04, 0.05, 0.06, 0.07, 0.08)

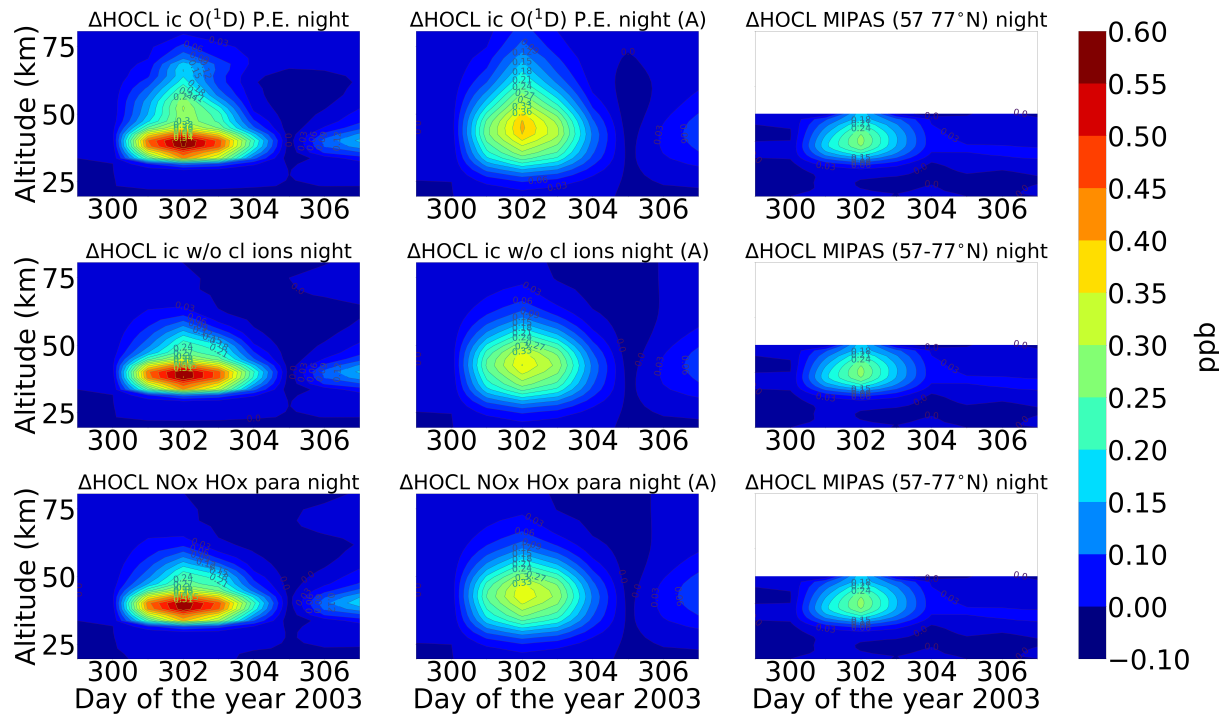


**Figure 6.** Same as figure 5 but for nighttime ( $\text{sza} > 98^\circ$ ). Colorbar interval: (-0.10, 0.00, 0.10, 0.15, 0.20, 0.25, 0.30, 0.35, 0.40, 0.45, 0.50, 0.55, 0.60)

### 3.3 ClONO<sub>2</sub> change

410 [Figure 6 shows](#) [Figures 7 and 8 show](#) the daily averaged absolute differences for [ENVISAT MIPAS V5 \(Höpfner et al., 2007a\)](#) and modelled chlorine nitrate w.r.t. 26<sup>th</sup> October 2003 for day-time and [night-time](#). The zonal average for ClONO<sub>2</sub> observations was also taken over a latitude range of 57-77°N, [which is at the edge the edge region](#) of the polar vortex. Continuous enhancements of ClONO<sub>2</sub> is observed for the full ion-chemistry model with peak values of 0.96 ppb and 1.15 ppb also approximately two days after the event for daytime and [night-time](#) respectively starting from the onset of the

415 event on 28<sup>th</sup> of October. The peak was observed around 25 km. In case of the model with full ion-chemistry but O(<sup>1</sup>D) [in set to](#) photo-chemical equilibrium, a peak value of around 0.18 ppb was observed for both day-time and [night-time](#) which compared much better with the MIPAS observations. Similar results were also observed for the sensitivity study without chlorine ion-chemistry and parameterised NO<sub>x</sub> and HO<sub>x</sub> model. The increase was seen also approximately two days after the event in the altitude range of 35-40 km. After the application of averaging kernels the peak value for the full ion-chemistry

420 daytime and [night-time](#) decreased down to 0.66 ppb and 0.78 ppb respectively. For the rest, the peak value decreased from 0.12 ppb to 0.09 ppb for daytime and from 0.18 ppb to 0.12 ppb for [night-time](#). Jackman et al. (2008) observed ClONO<sub>2</sub> maximum enhancements of 0.3-0.4 ppb with the peak production at a higher altitude of 40-45 km with WACCM3. The peak however was produced several days later than MIPAS. The application of MIPAS averaging kernels moved the peak

down to 40 km and the predicted peak increases are reduced substantially to about 0.2 ppbv, about a factor of 2 less than MIPAS observations.

The enhanced ClONO<sub>2</sub> production happens due to SPE produced NO<sub>x</sub> via ~~reaction~~ Reaction R32. ClONO<sub>2</sub> is removed mainly by photolysis in the sunlit atmosphere and, to a lesser extent, by reaction with atomic oxygen. And due to its pressure dependence, ClONO<sub>2</sub> formation by Reaction R32 is more effective at lower altitudes (Funke et al., 2011). The zonal average of MIPAS observations were tested for latitude bands 57-77°N, i.e., at the edge ~~region~~ of the polar vortex and 70-90°N, deep in the polar vortex. The sample of 57-77°N works better for the inter-comparison of ClONO<sub>2</sub> compared to 70-90°N. In case the sample is taken deep in the vortex, the model seemed to fairly underestimate the peak values. This can be explained by the ~~reaction~~ Reaction R32, where formation of ClO needs sunlight, which is again available more at the edge ~~region~~ of the polar vortex. But ClONO<sub>2</sub> can also photolyse in the presence of sunlight ~~-Due and due~~ to this, there is a balance between the two processes and ClONO<sub>2</sub> can form at the edge ~~of the polar vortex region~~ which can be transported deep into the vortex and conserved there at high latitudes. This however cannot be reproduced by the 1D model because it is fixed at a certain location and has no transport.

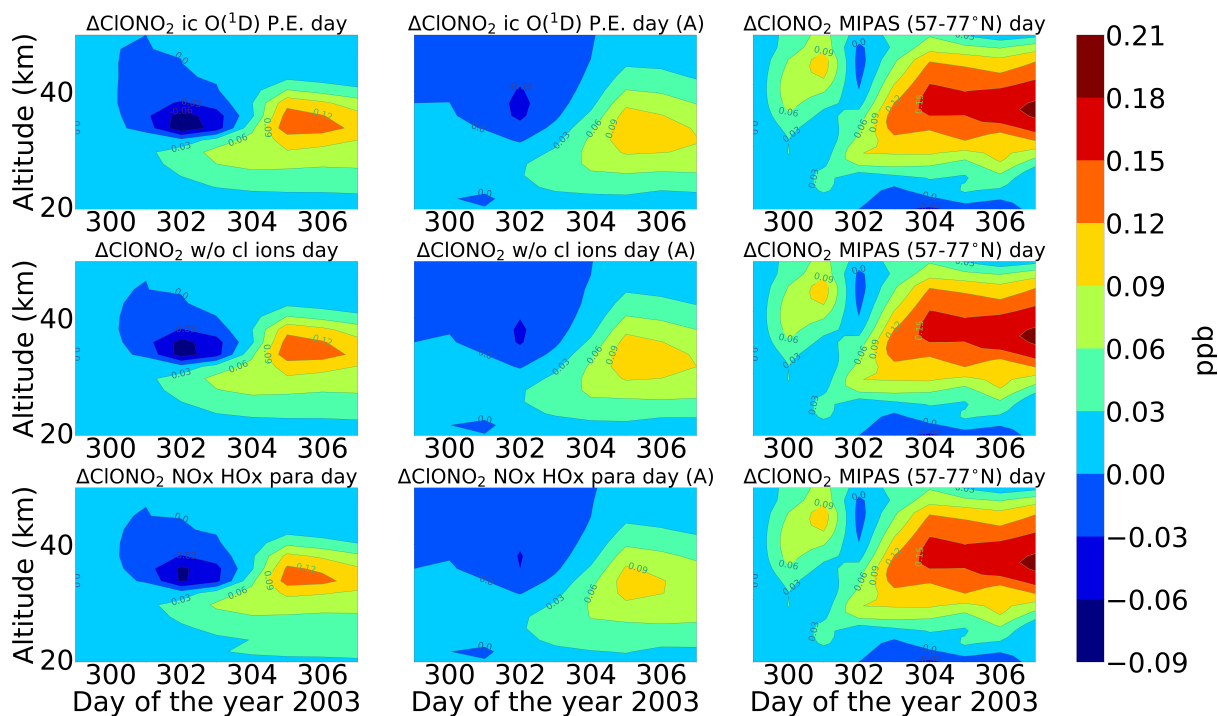


**Figure 7.** Same as figure 5 but for ClONO<sub>2</sub>. Colorbar interval: (-0.09, -0.06, -0.03, 0.00, 0.03, 0.06, 0.09, 0.12, 0.15, 0.18, 0.21)

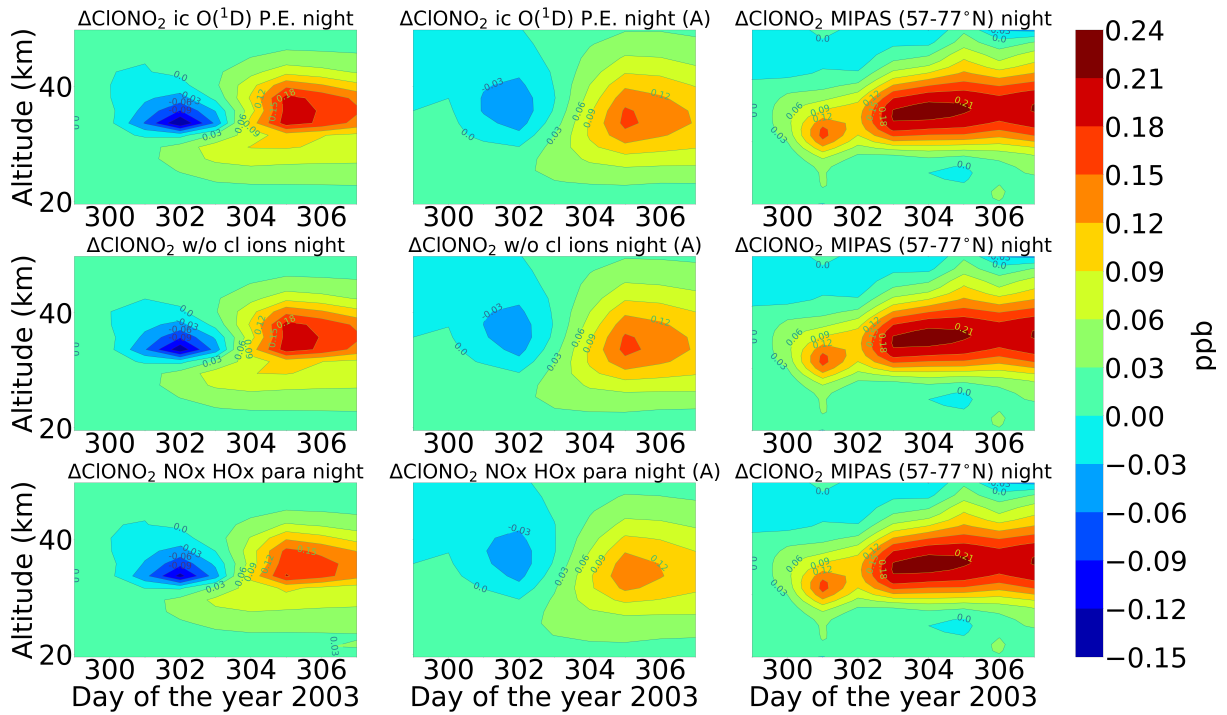


**Figure 8.** Same as figure 6 but for ClONO<sub>2</sub>. Colorbar interval: (-0.15, -0.12, -0.09, -0.06, -0.03, 0.00, 0.03, 0.06, 0.09, 0.12, 0.15, 0.18, 0.21, 0.24)

### 3.4 Odd oxides of nitrogen (NO<sub>y</sub>)

An important impact of proton precipitation in the middle atmosphere is the formation of NO<sub>x</sub> which happens by the dissociation of molecular nitrogen by ionisation and subsequent recombination with oxygen. In order to assess the agreement of the  
 440 ~~observed~~ [ENVISAT MIPAS V5 \(Funke et al., 2005\)](#) and modelled SPE related odd nitrogen enhancements, total NO<sub>y</sub> (=NO + NO<sub>2</sub> + HNO<sub>3</sub> + 2N<sub>2</sub>O<sub>5</sub> + ClONO<sub>2</sub>) is compared. The observed and modelled NO<sub>y</sub> enhancements w.r.t. 26<sup>th</sup> October is shown in [figure 7 for daytime \(left\) and night-time \(right\)](#) [figures 9 and 10 for daytime and nighttime](#) conditions respectively. Averaging kernels are also applied to the model profiles for the different NO<sub>y</sub> species for the different model settings and then added, except for NO. In case of MIPAS NO and NO<sub>2</sub> data, there is a complication which is, that instead of mixing ratios  
 445 the logarithms of the mixing ratios are retrieved; also the averaging kernels refer to the logarithms of the mixing ratios. The application of MIPAS averaging kernels to a better resolved profile on the basis of the coarse-grid averaging kernel **A** of the logarithm of the mixing ratio then is (Stiller et al., 2012):

$$x_{\text{new}} = \exp(\mathbf{A} \log(x_{\text{orig}}) + (\mathbf{I} - \mathbf{A}) \log(x_a)) \quad (3)$$

There is a general issue with logarithmic retrievals, because regularization is self-adaptive and depends on the actual state  
 450 of the atmosphere. For an SPE response, if the NO peaks around 50-60 km and if there is a better sensitivity at this altitude the

Jacobian and the averaging kernels scale with the volume mixing ratio. For  $\text{NO}_2$  however, the logarithmic averaging kernels behave well and are not dependent on the actual conditions (for a deeper discussion of the problem of time and state dependent averaging kernels, see von Clarmann et al. (2020)). Due to this complication, for the total  $\text{NO}_y$  in the second column of [figure 7-figures 9 and 10](#) for both daytime and [night-time](#), NO is added without the application of the averaging kernels as compared to the rest of the species.

The magnitude of  $\text{NO}_y$  enhancements is found to be larger for the ExoTIC model with ion-chemistry settings compared to the MIPAS observations for both daytime and [night-time](#). However the SPE induced  $\text{NO}_y$  layer is reproduced well in terms of vertical distribution. The MIPAS observations showed a production of 30-40 ppb in the upper stratosphere during [night-time](#) and 20-30 ppb during day-time. The [MIPAS observations show much higher dynamics than ExoTIC for both day-time and nighttime. The nighttime values show stronger dynamics with decreased ionisation rates on day 305-306 and connected to this less  \$\Delta\text{NO}\_y\$  reaches a constant state after the maximum of the first SPE on day 303. This could be an indication that some of the  \$\text{NO}\_y\$  recombination speeds are faster than expected.](#) The results are shown upto 50 km since above 50 km NO is the largest contributor ([Funke et al., 2011](#)) and averaging kernels are not applied to NO. Another reason is that large uncertainties of small vmr values of  $\text{ClONO}_2$  ([Höpfner et al., 2007b](#)) will spoil the  $\text{NO}_y$  sum and it's uncertainty. The [night-time](#) results compare better with the observations, specially for the parameterised  $\text{NO}_x$  and  $\text{HO}_x$  model. For day-time, the model with and without [AK-averaging kernel \(A\)](#) didn't make too much of a difference because NO was added without [AK-averaging kernel \(A\)](#) and was abundant during daytime.

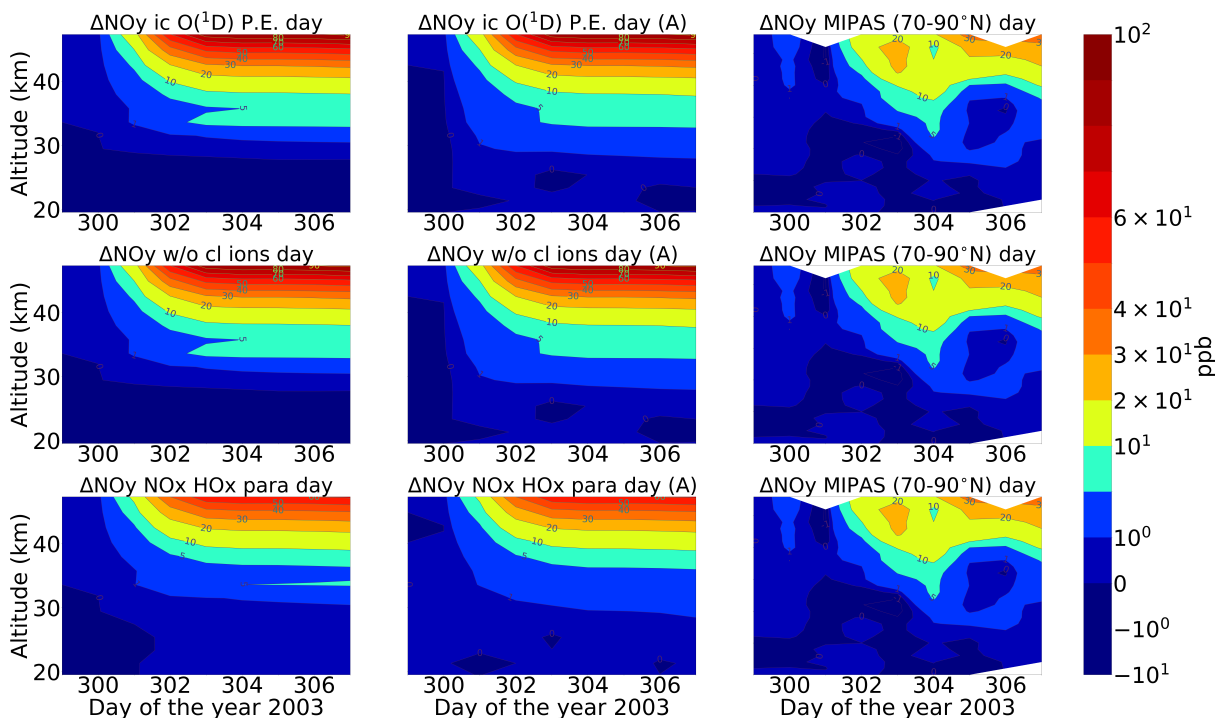


**Figure 9.** Same as figure 5 but for  $\text{NO}_y$  species. Colorbar interval:  $(-10^{-1}, -10^0, 0, 10^0, 10^1, 2*10^1, 3*10^1, 4*10^1, 6*10^1, 10^2)$

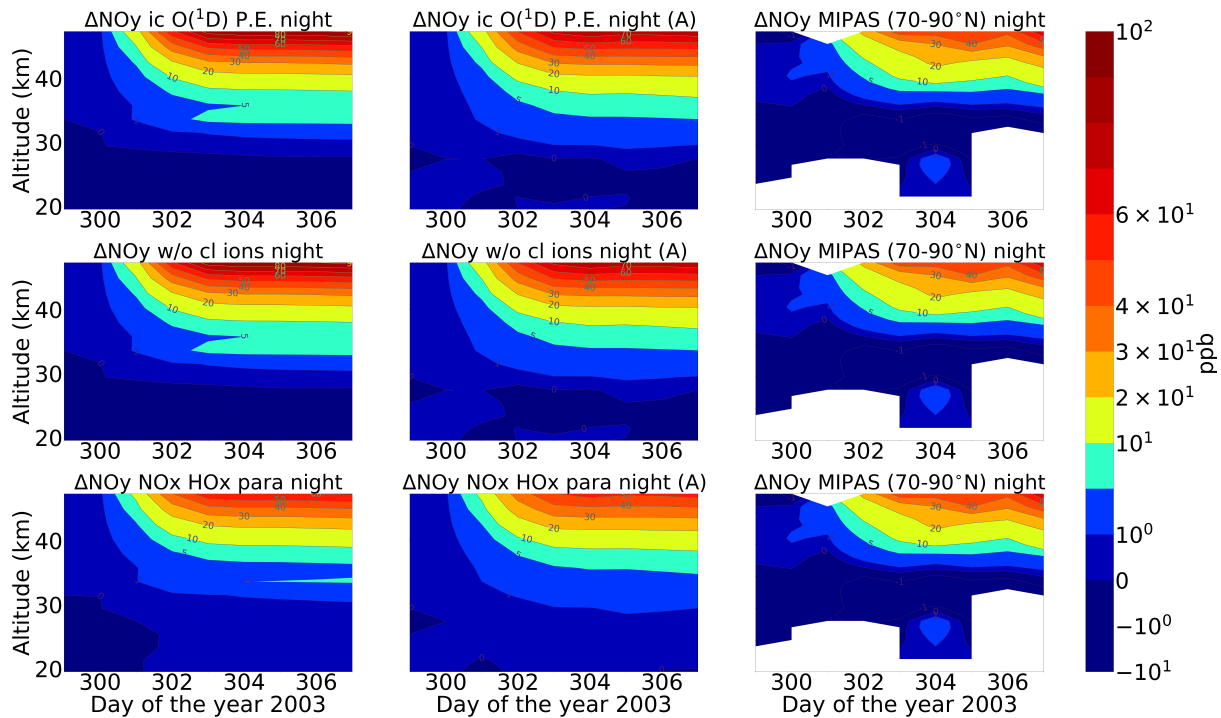


**Figure 10.** Same as figure 6 but for  $\text{NO}_y$  species. Colorbar interval:  $(-10^{-1}, -10^0, 0, 10^0, 10^1, 2 \times 10^1, 3 \times 10^1, 4 \times 10^1, 6 \times 10^1, 10^2)$

### 3.5 Ozone

470 Energetic particles in the polar atmosphere enhances the production of  $\text{NO}_x$  and  $\text{HO}_x$  in the winter stratosphere and meso-  
 sphere. Both  $\text{NO}_x$  and  $\text{HO}_x$  are powerful ozone destroyers. An important aspect in the evaluation of the ability of models is the  
 reproduction of the observed ozone destruction caused by the catalytic cycles of  $\text{NO}_x$  and  $\text{HO}_x$  during SPE induced chemical  
 composition changes. As inferred from observations, stratospheric ozone decreases due to the indirect effect of EPP by about  
 10–15 % as observed by satellite instruments (Meraner and Schmidt, 2018). López-Puertas et al. (2005) found  $\text{HO}_x$  related  
 mesospheric ozone losses upto 70% and  $\text{NO}_x$  related stratospheric loss of around 30% during the Halloween SPE.  
 475 ~~Figure 8 shows observed and~~ Figures 11 and 12 show ENVISAT MIPAS V5 (Glatthor et al., 2006) and modelled temporal  
 evolution of the relative ozone changes w.r.t. 26<sup>th</sup> October, averaged over 70-90°N for daytime (left) and night-time (right) and  
 nighttime respectively. For ozone, the long term history of air parcels is more important as air parcels that are ozone depleted  
 gets dispersed into the mid-latitudes if they are at the edge region of the vortex. So a sample deeper in the vortex for ozone is  
 better, the reason we chose 70-90°N here. A loss of 60-75 % is observed during the event itself in the mesosphere that is short  
 480 lived and is related to the  $\text{HO}_x$  catalytic cycle (Reactions R6, R7, R9 and R10, (Funke et al., 2011)(Bates and Nicolet, 1950).  
 ). The ozone recovers after the event, since  $\text{HO}_x$  is short-lived. A second peak is observed on the 3rd of November which is  
 related to a weaker coronal mass ejection event.  $\text{NO}_x$  related loss of 15 % is observed in the stratosphere that lasts longer and  
 is also related to the polar winter atmosphere (Reactions R12 and R13). The full ion-chemistry shows an ongoing loss of 45



% starting from the event day and the sensitivity study with  $O(^1D)$  in photo-chemical equilibrium confirmed that this loss is  
 485 due to ~~reactions~~ Reactions like R40 and R37, which produces OH and Cl contributing further to ozone loss. The agreement  
 between the observations and the model results, for ~~night-time~~ nighttime, for the three model results except for the full ion-  
 chemistry is excellent in the mesosphere indicating a good ability of the model to reproduce  $HO_x$  related ozone loss for SPEs.  
 However, the ozone loss shifted to lower altitudes for both daytime and nighttime in all the model settings as compared to  
 MIPAS observations. This could be explained as a result of the AISstorm ionisation rates that was used in the model which  
 490 could be different to what MIPAS might have experienced during the SPE. AISstorm here uses proton fluxes from GOES  
 10 and the ionisation rates should be a lower estimate. The SPE ionisation happens in the denser atmosphere, therefore the  
 conversion from particle fluxes into ionisation should be more or less precise in terms of total ionisation and altitude. The main  
 uncertainty of SPE ionisation in AISstorm is the size of the area that is affected by high energetic particle precipitation. This  
 cannot be derived from these channels but is taken from a lower energy channel on another satellite and thus it might be an  
 495 underestimate of the polar cap size. However if that would be important for the spatial average 70-90°N, we should see an  
 underestimation of the ionisation (and  $NO_y$ ) as well, which doesn't seem to be the case (and which is unlikely anyway as the  
 equatorward boundary should be at about 60°N).

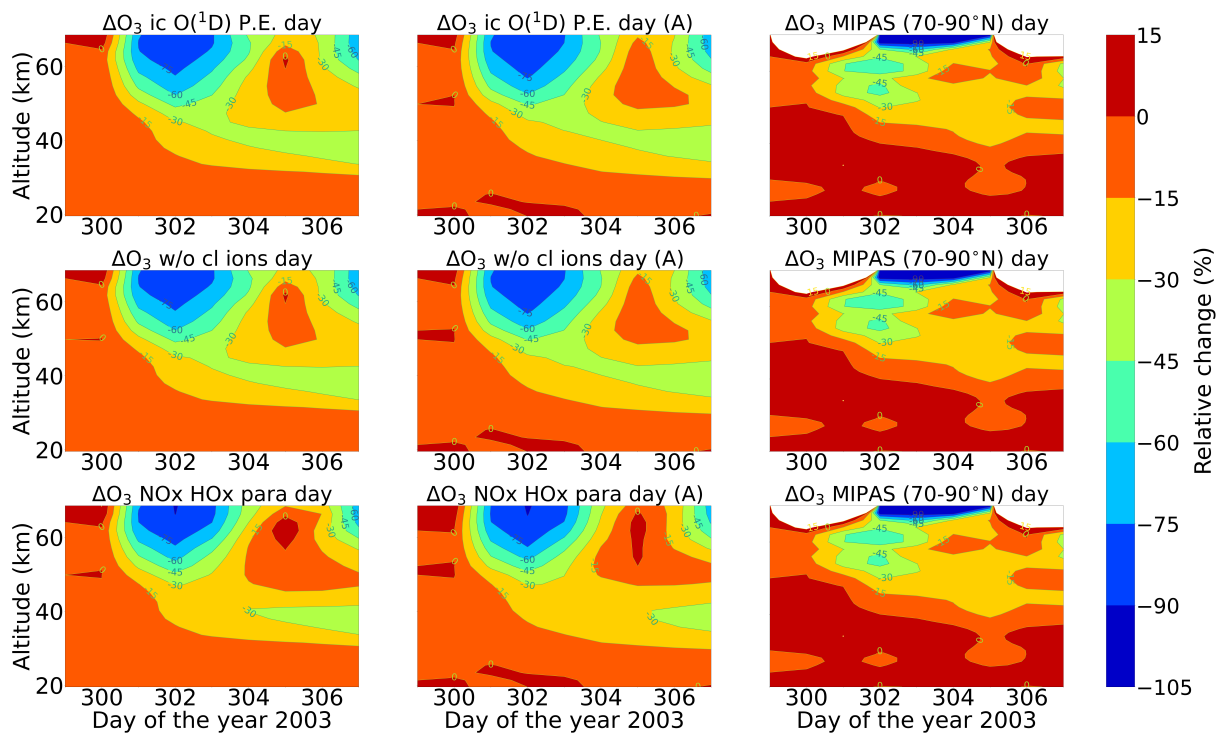


**Figure 11.** Relative difference of ozone w.r.t. 26<sup>th</sup> October. Rest is same as Figure 5. Colorbar interval: (-105, -90, -75, -60, -45, -30, -15, 0, 15)

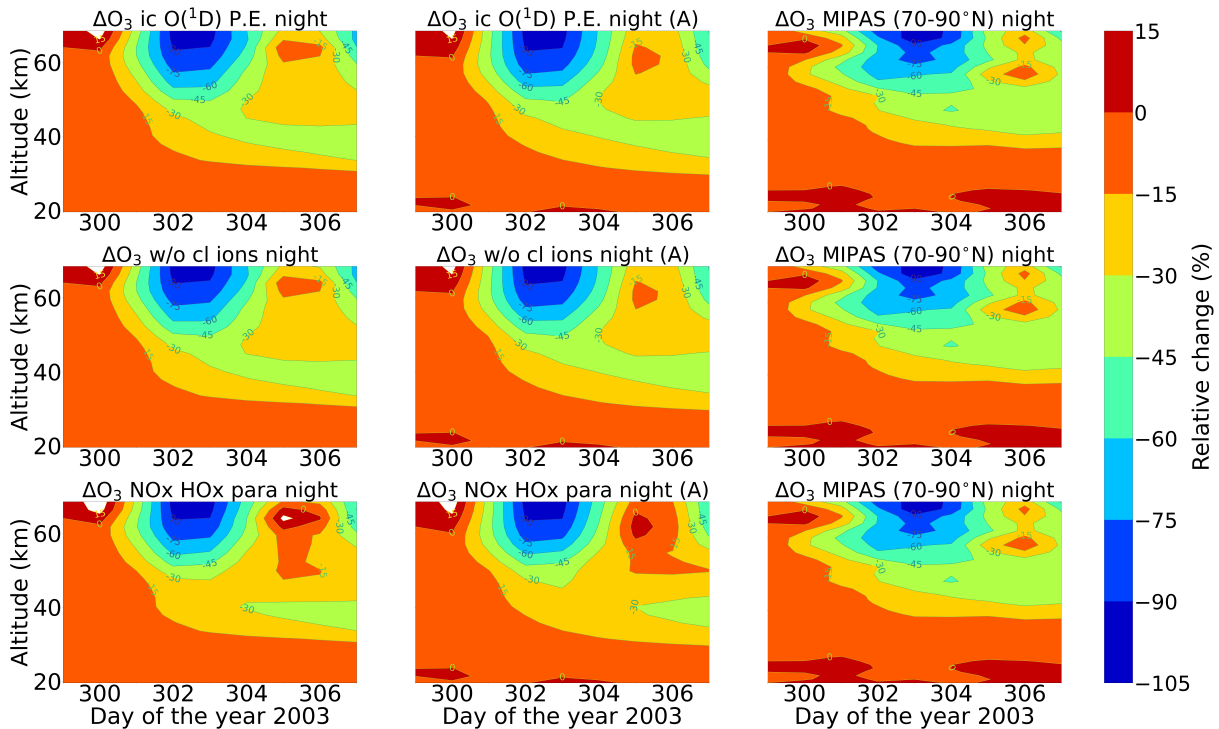


**Figure 12.** Same as figure 11 but for nighttime. Colorbar interval: (-105, -90, -75, -60, -45, -30, -15, 0, 15)

#### 4 Comparison of the Halloween storm and the extreme solar event of 775 A.D.

In this section, a comparison study between the Halloween storm of 2003 and an extreme event of 775 A.D. is presented. The model simulations [are performed at a latitude of 67.5°N and](#) begin at the noon of 27<sup>th</sup> October (day 300) [and the](#) [The](#) ionisation rate profiles [are](#) obtained from AISstorm for both the events [and](#) are input from the noon of October 28 to noon of October 29. Since the studies were performed without horizontal and vertical transport, the results shown here are restricted to a short time period. The results are shown for the model simulations for the settings that compared well with MIPAS observations.

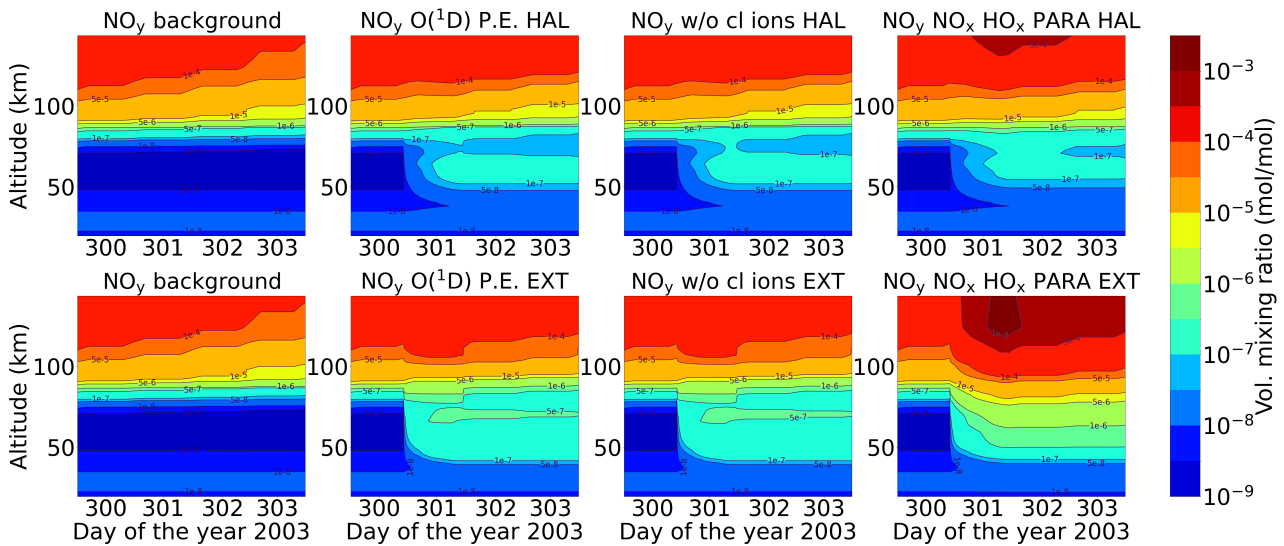
##### 4.1 $\tilde{\text{NO}}_y$ and $\text{HO}_x$ :

Figure 9-13 shows the formation of  $\tilde{\text{NO}}_y$  during the Halloween SPE and the extreme scenario with different settings of the ion-chemistry.  $\tilde{\text{NO}}_y$  consists species of odd nitrogen as shown in equation 4:

$$\tilde{\text{NO}}_y = \text{NO} + \text{NO}_2 + \text{N} + \text{HNO}_3 + 2\text{N}_2\text{O}_5 + \text{NO}_3 + \text{ClONO}_2, \quad (4)$$

After the onset of the event,  $\tilde{\text{NO}}_y$  starts accumulating over time in the stratosphere and lower mesosphere. For the extreme scenario, the volume mixing ratio (VMR) of  $\tilde{\text{NO}}_y$  is about one order of magnitude larger compared to the Halloween SPE in the upper stratosphere and lower mesosphere. For example, the amount of  $\tilde{\text{NO}}_y$  at 60 km is found to be 50 ppb for the

Halloween event compared to 500 ppb for the extreme event. Additionally for the extreme event,  $\tilde{\text{NO}}_y$  is seen to be formed even in the lower stratosphere (below 30 km). This is because of the high values of ionisation rates that reached further down in altitude in this case. A small difference was observed between the sensitivity study without the chlorine ion-chemistry and the model setting of ion-chemistry with  $\text{O}(^1\text{D})$  in photo-chemical equilibrium around 75 km. The full ion-chemistry and the ion-chemistry setting  $\text{O}(^1\text{D})$  to photo-chemical equilibrium didn't show much of a difference. For the parameterised model,  $\tilde{\text{NO}}_y$  enhancements are observed in the mesosphere and lower thermosphere with higher values seen for the extreme scenario compared to the Halloween event. Since only N, NO and  $\text{NO}_2$  are present for the parameterised  $\text{NO}_x$ , the impact of the scavenging ~~reaction R2~~ Reaction, R2 is stronger and the partitioning between N and NO is different compared to the ~~full~~ ion chemistry which also contains other  $\tilde{\text{NO}}_y$  species like  $\text{HNO}_3$  etc. ~~R2-R2~~ R2-R2 drives the  $\text{NO}_x$  parameterisation and makes the main difference w.r.t. the ion-chemistry. ~~The~~ In contrast to our results, which show the total  $\text{NO}_y$  that includes  $\text{NO}_x = \text{N} + \text{NO}$ , Andersson et al. (2016) showed that WACCM-D with the D-region ion-chemistry predicts more  $\text{NO}_x$  in the mesosphere compared to WACCM with the standard parameterisation of  $\text{NO}_x$  and  $\text{HO}_x$  production for the northern polar cap region, latitude  $> 60^\circ\text{N}$  during the SPE of January 2005. Kalakoski et al. (2020) also reported the same when considering SPEs using proton flux data from satellite-based GOES observations. They considered an event in which the peak proton flux exceeded 100 particle flux units (pfu), with pfu defined as the 5 min average flux in units of particles  $\text{cm}^{-2}\text{s}^{-1}\text{sr}^{-1}$  for protons with energy larger than 10 MeV. The rate of formation of  $\text{NO}_x = \text{N} + \text{NO}$  is indeed higher in the mesosphere when full ion-chemistry is considered, but the partitioning between the formation of N and  $\text{N}(^2\text{D})$  forming NO is also increasingly in favour of N, meaning that the rate of loss of NO is also faster in this altitude range when full ion-chemistry is considered. This can lead to less NO depending on the absolute rate of  $\text{NO}_x$  formation, and the partitioning between N and NO in this formation. The  $\text{HO}_x$  parameterisation doesn't make much of a difference for  $\tilde{\text{NO}}_y$ .

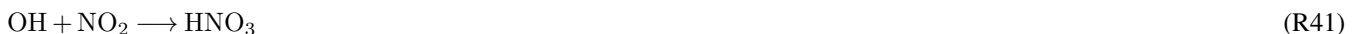


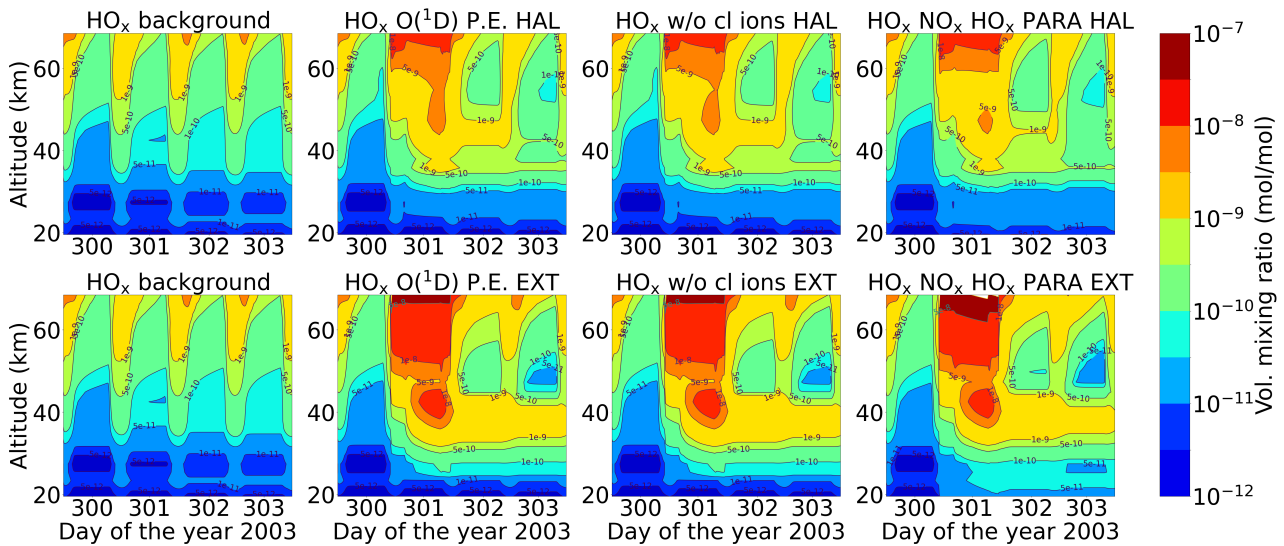
**Figure 13.** Comparison of the Halloween SPE and the extreme scenario (row-wise) for  $\tilde{\text{NO}}_y$ : reference run (background atmosphere), full ion-chemistry with  $\text{O}(^1\text{D})$  set to photo-chemical equilibrium, without chlorine ions and parameterised  $\text{NO}_x$  and  $\text{HO}_x$  model (column-wise) for a high latitude of  $67.5767.5^\circ\text{N}$ .

Figure 14 shows the temporal evolution of  $\text{HO}_x$  for the Halloween SPE and extreme scenario that consists of odd hydrogen species (equation 5);



$\text{HO}_x$  was not shown for the MIPAS comparison due to the fact that H and OH are not provided by MIPAS.  $\text{HO}_x$  enhancements are seen during the event. For the Halloween SPE,  $\text{HO}_x$  enhancements of 0.1 ppm were observed in the mesosphere during the event whereas for the extreme scenario these enhancements were seen to penetrate deep down. However after the event stops, the  $\text{HO}_x$  disappears at higher altitudes, since it is short-lived up there. But at lower altitudes, around 25-40 km,  $\text{HO}_x$  enhancements of around 1 ppb was found to be continuous and more persistent, specially for the extreme scenario. The full ion-chemistry shows  $\text{HO}_x$  enhancements below 30 km which is due to the presence of  $\text{O}(^1\text{D})$ , that can react with water vapour, hydrogen and methane via Reactions R37, R38 and R39. However with  $\text{O}(^1\text{D})$  set to photo-chemical equilibrium, the  $\text{HO}_x$  enhancements below 30 km disappeared for both the events. The impact of chlorine ion-chemistry is seen to be rather small. For the parameterised model, the recovery of  $\text{HO}_x$  after the event was found to be slower compared to the ion-chemistry model. The full high values of  $\text{HO}_x$  are balanced by the continuous destruction of water vapour and when it is completely destroyed, the  $\text{HO}_x$  formation breaks down. So the full parameterisation with both  $\text{NO}_x$  and  $\text{HO}_x$  is different but the water vapour is a limiting factor for both. The full ion-chemistry with more  $\text{HO}_x$  can also lead to a faster reaction between OH and  $\text{NO}_2$  (R41), which can produce  $\text{HNO}_3$  contributing a difference to the recovery of  $\text{HO}_x$ .





**Figure 14.** Same as Figure 13 but for odd hydrogen species,  $\text{HO}_x$ .

## 4.2 Chlorine species:

Figure 15 shows the volume mixing ratios of HCl for the two events. Loss of HCl, which can occur via transformation into reactive chlorine as it is taken up from the gas phase into negative ions, is seen during the event in both cases, pronounced more for the extreme scenario. This occurred both in the stratosphere and the mesosphere for full ion-chemistry. Negative ions upon reaction with HCl can form  $\text{Cl}^-$  ions, which forms large cluster ions thereby releasing Cl upon recombination (Sinnhuber et al., 2012),



where  $\text{X} = \text{O}, \text{O}_2, \text{CO}_3, \text{OH}, \text{NO}_2, \text{NO}_3$ ;  $\text{Y} = \text{HCl}, \text{H}_2\text{O}, \text{CO}_2$  and  $\text{Z} =$  positive ions (Kopp and Fritzenwallner, 1997).  $\text{Cl}^-$  and  $\text{Cl}^-$  cluster ions like  $\text{Cl}^-(\text{H}_2\text{O})$  can also release HCl via reaction with H (Kopp and Fritzenwallner, 1997). HCl can react with  $\text{O}(^1\text{D})$  via Reaction R40 resulting in an enhanced loss of HCl below 40 km but that disappears when  $\text{O}(^1\text{D})$  is set to photo-chemical equilibrium. At 40-50 km, ExoTIC with ion-chemistry and  $\text{O}(^1\text{D})$  set to photo-chemical equilibrium observed 5-15% HCl loss for the Halloween SPE and 20-45% HCl loss for the extreme event. From the sensitivity study without the chlorine ions, it is evident that the huge loss of HCl, around 75% observed in the mesosphere is due to the same chlorine ion-chemistry. The parameterised model underestimates the loss of HCl which was also found in studies by Winkler et al. (2009).

The primary neutral reaction that leads to the decrease in HCl below 50 km is a series of reactions involving  $\text{HO}_x$  species that are part of the catalytic ozone destruction cycle (Reactions R6 and R7). The decrease in ozone concentration has a secondary effect on the concentration of HCl. In the absence of an SPE, ozone plays a role in the conversion of ClO back to HCl.

565 However, during an SPE, the enhanced ionisation and subsequent formation of ions disrupt this ozone destruction and formation cycle. This leads to an increase in the concentration of ClO and a subsequent reduction in the concentration of HCl. The excess ClO can further participate in additional ozone depletion cycles, leading to a decline in ozone levels during the event. Andersson et al. (2016) reported daily averaged anomalies of HCl in both hemispheres for the latitudinal band 60–82.5°N at altitudes between 40 and 52 km. They compared WACCM-D consisting of the D-region ion-chemistry and WACCM consisting of the standard NO<sub>x</sub> and HO<sub>x</sub> parameterisation with MLS observations. They found a rapid HCl decrease of about 2-6% during the January 2005 SPE in both hemispheres. With WACCM-D, a loss of around 4% was found compared to a loss of 3% in standard WACCM in the Northern Hemisphere. They also showed that WACCM-D showed better agreement with MLS observations.

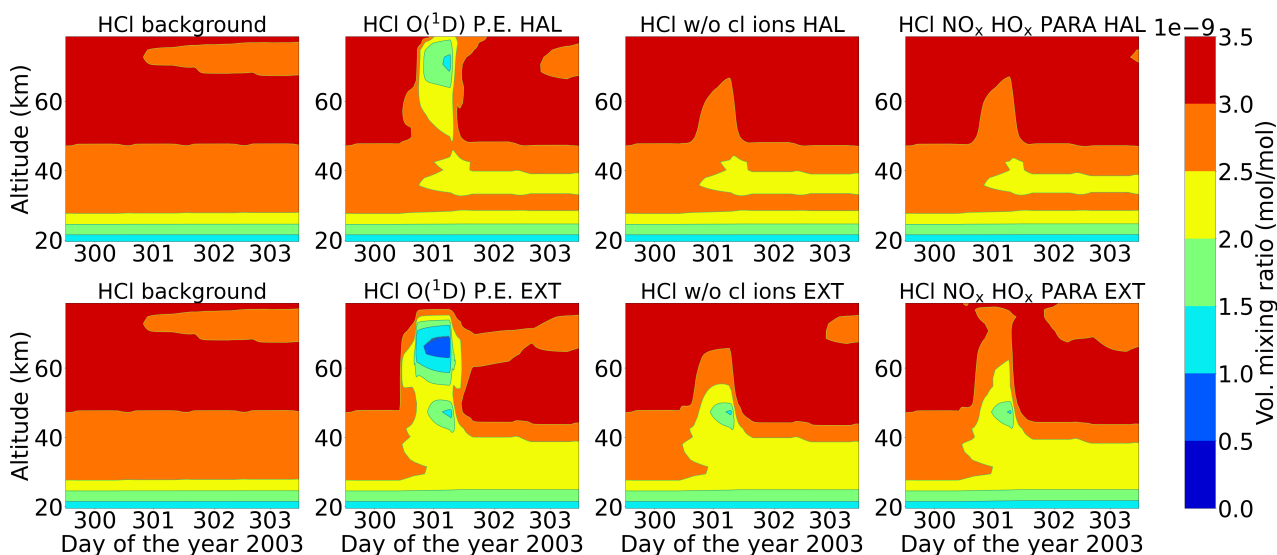
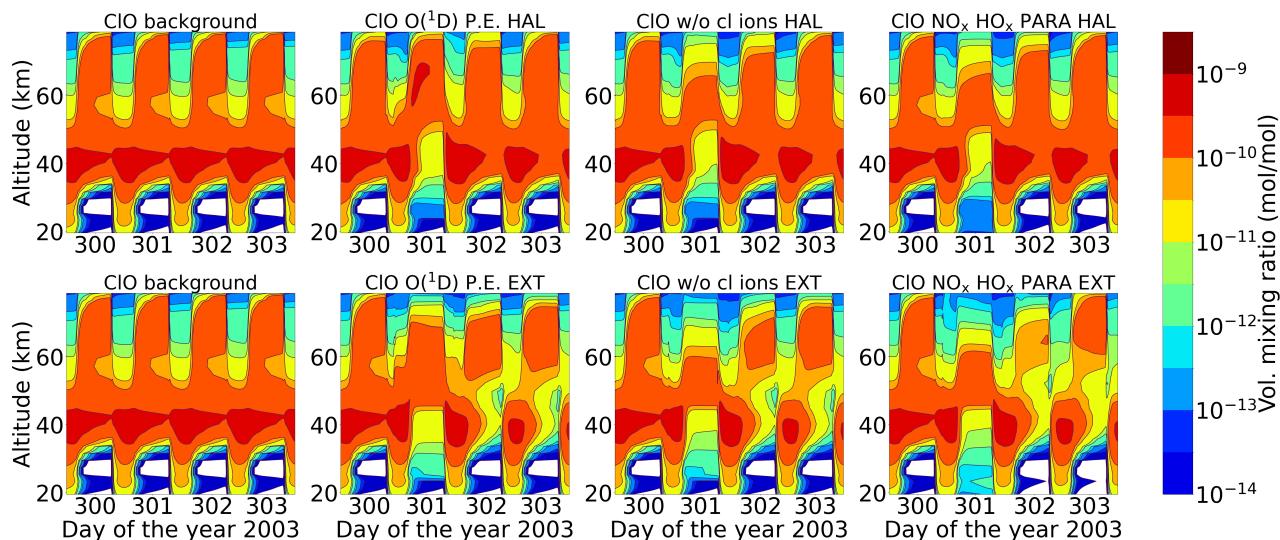


Figure 15. Same as Figure 13 but for HCl

575 Since  $\tilde{\text{NO}}_y$  and HO<sub>x</sub> production is enhanced during SPEs, which is evident from figures 9 and 10, 13 and 14, they can react with reactive chlorine species like ClO. ClO can either react with HO<sub>x</sub> producing short term enhancement in HOCl (R19), or with NO<sub>x</sub> slowly producing ClONO<sub>2</sub> (R32). ClO is formed from the reactive Cl via Reaction R7-R21 by neutral gas phase reactions of Cl with ozone in the altitude range of 35-40 km. ClO can react with HO<sub>x</sub> and NO<sub>x</sub> species to form HOCl and ClONO<sub>2</sub> (reactions R8 and R13).

580 From figure 12, 16, it can be seen that ClO decreases during the event for the same altitude range but recovers straight after the event stops. ClO can react with HO<sub>x</sub> species during SPEs, particularly HO<sub>2</sub> to produce HOCl (R19), which is also a short-lived species. Therefore, a short term enhancement of HOCl is seen during both the events (Figure 13, figure 17) which was also observed by von Clarmann et al. (2005) for the Halloween SPE. However, for the extreme scenario, loss of ClO continues specially around 30-40 km even after the event stops. This is because of the excess HONO<sub>x</sub> available for the extreme event ; also at the same altitude range, due to which R8-R32 can happen continuously. And loss of HOCl is also which is supplemented

by an increase in  $\text{ClONO}_2$  after the extreme event as seen from figure 18. Loss of HOCl seen after the extreme event which is due to excess  $\text{HO}_x$  as well. HOCl can react with OH to form ClO (R9R24) and then ClO can react back with  $\text{HO}_2$  and this catalytic cycle thereby results in the loss of both species due to excess  $\text{HO}_x$ .



**Figure 16.** Same as figure 15 but for ClO

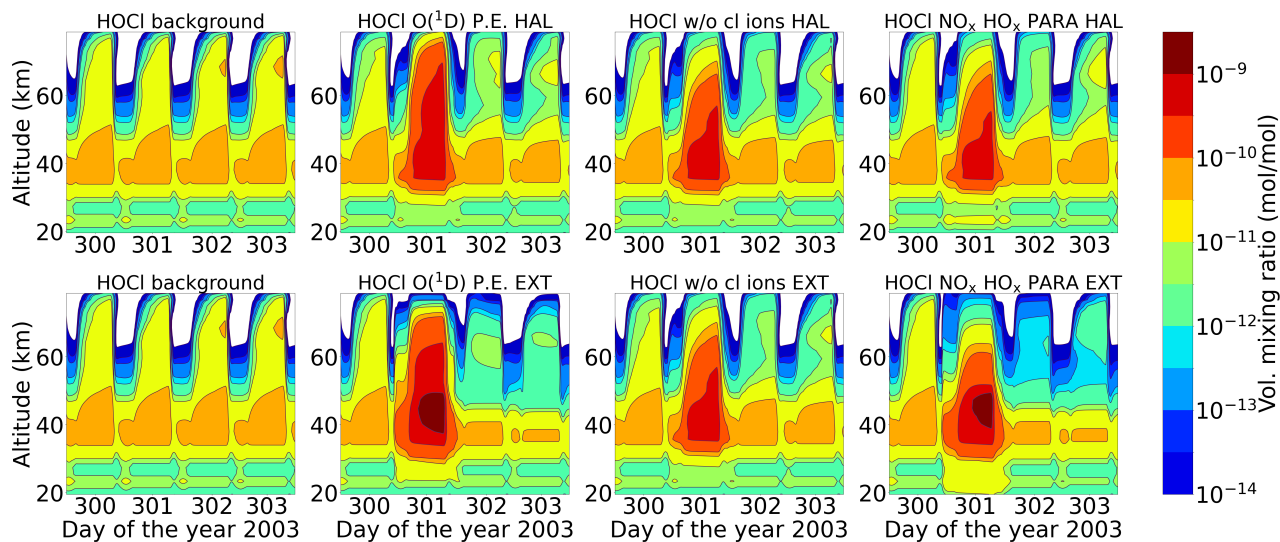


**Figure 17.** Same as figure 15 but for HOCl

An increase in  $\text{ClONO}_2$  is also observed during both the events at an altitude of 60 km (Figure 14 figure 18). Solomon et al. (1981) pointed out that the increasing  $\text{NO}_x$  concentrations after a SPE interact with chlorine species, forming chlorine nitrate

at the expense of reactive radicals. This reaction is of importance in the lower and middle stratosphere around 40 km, (Jackman et al., 2000) but not so important at higher altitudes. It can be seen from [Figure 14](#) [figure 18](#) that at an altitude of 40 km, ClONO<sub>2</sub> increases after the event has stopped. This is because ~~during~~ after the event ClO is lost via ~~R8 and Reaction R32~~ since NO<sub>x</sub> is formed slowly accumulating over time. So the formation of ClONO<sub>2</sub> via ~~R13-R32~~ R13-R32 is slow, hence leading to high production after the event in the lower and middle stratosphere. The chlorine ion-chemistry plays a small role for ClONO<sub>2</sub> around 45-50 km specially during nighttime on day 301. The production of ClONO<sub>2</sub> when the chlorine ion-chemistry is switched off is comparatively higher at that altitude.

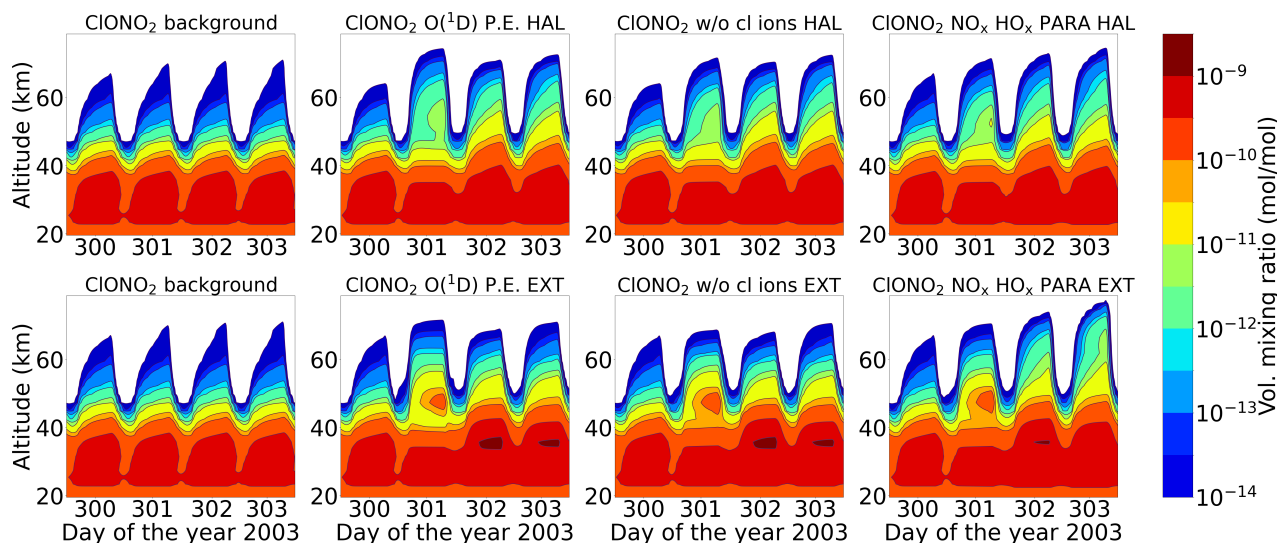


**Figure 18.** Same as figure 15 but for ClONO<sub>2</sub>

595 Figure [15-19](#) shows the chlorine species at an altitude of 40 km for the various model set-ups. There is a small impact of chlorine ion-chemistry on the loss of HCl, whereas the parameterised NO<sub>x</sub> and HO<sub>x</sub> underestimates it. ClO decreases during the event and transfers to HOCl via ~~reaction R8~~ Reaction R19. After the event, it recovers and the HOCl enhancements also decrease. For the extreme event however, ongoing loss of ClO during ~~night-time~~ nighttime is observed which is due to the excess HO<sub>x</sub> produced during the extreme event. Reformation of HCl after the event is observed that happens via Reactions  
 600 ~~R11 and R12~~ R26 and R27.



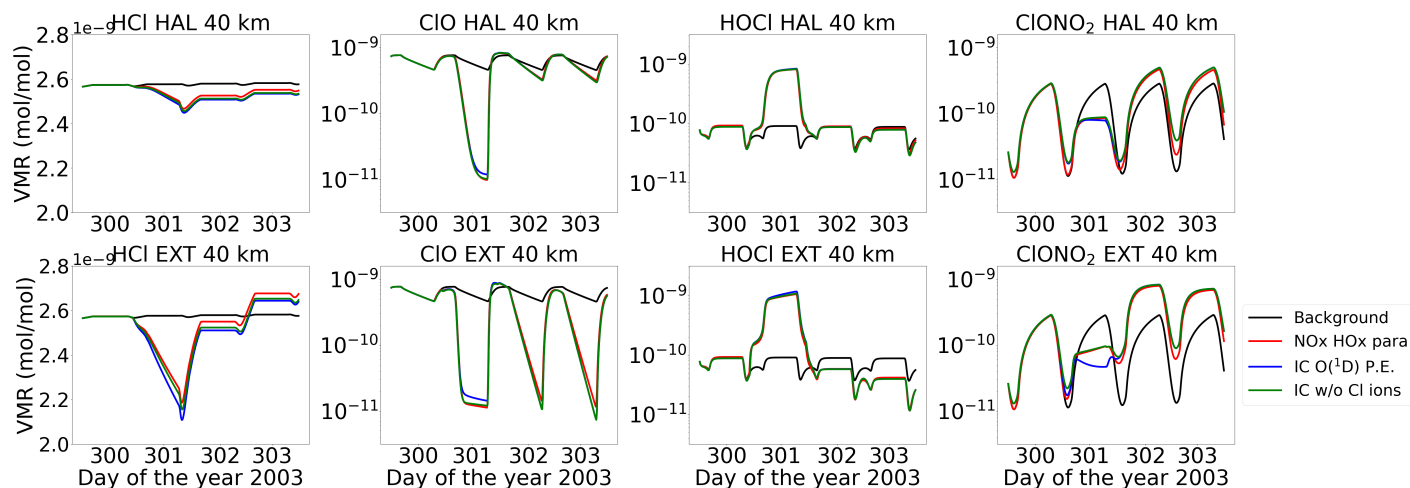


**Figure 19.** Comparison of the Halloween SPE and the extreme scenario for (column wise): HCl, ClO, HOCl and ClONO<sub>2</sub> at 40 km.

An interesting observation for HCl can be seen from the figure 15-19 for the extreme scenario, where the recovered HCl after the event shows a positive excursion. This depends on the diurnal cycle of ClO and happens mainly during night time. The reformation of HCl can happen via [R11 and R12 Reactions R26 and R27](#) during night time because during daytime HO<sub>2</sub> and H<sub>2</sub>O<sub>2</sub> photolyses. This can be seen from the figure 16-20 where HO<sub>2</sub> and H<sub>2</sub>O<sub>2</sub> production increases during the event mainly at night time. ~~Since the chlorine atoms aren't enough during night time (also seen from the first plot of figure 16), a~~ steep increase in HCl is observed during the transition from day to night ~~where Cl, HO<sub>2</sub> and H<sub>2</sub>O<sub>2</sub> increases which is constant over the night and increases again afterwards at the beginning of the day. This is due to the fact that during nighttime the concentration of free chlorine atoms is typically low since the primary source of these atoms is the dissociation of chlorine-containing reservoir species, such as chlorine nitrate (ClONO<sub>2</sub>). ClONO<sub>2</sub> occurs predominantly during daytime due to the presence of sunlight, where it is photolysed to release chlorine atoms and hence at sunrise this renewed increase in chlorine atoms results in a subsequent increase in HCl levels.~~

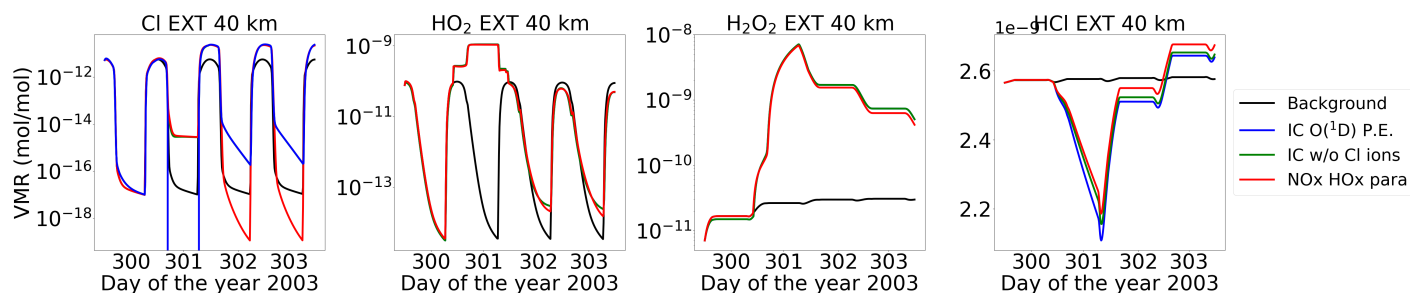


**Figure 20.** Volume mixing ratios of species (Cl, HO<sub>2</sub>, H<sub>2</sub>O<sub>2</sub> and HCl) at 40 km for the extreme event. The different lines are for the model settings: reference (black), ion-chemistry with O(<sup>1</sup>D) in photo-chemical equilibrium (blue), without chlorine ions (green) and parameterised NO<sub>x</sub> and HO<sub>x</sub> (red)

### 4.3 Ozone:

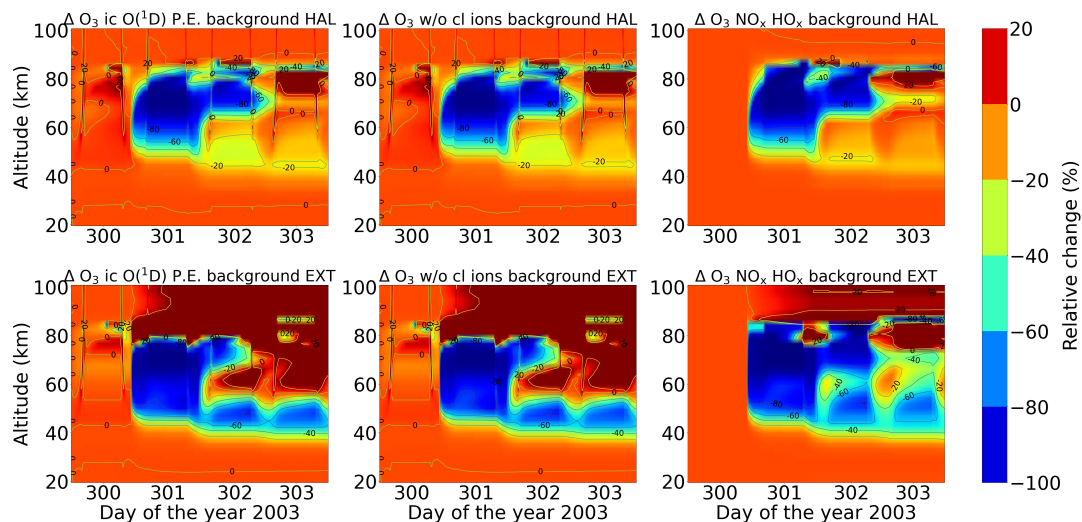


**Figure 21.** Percentage difference of ozone for the different model runs w.r.t. the reference run (row-wise): Halloween event and extreme scenario; (column-wise): ion-chemistry with  $O(^1D)$  in photochemical equilibrium, without Cl ions and parameterised  $NO_x$  and  $HO_x$ .

Figure 17-21 shows the percentage difference of ozone for the two events for the different model runs calculated w.r.t. the reference run. It is seen that with the onset of the event, ozone is completely lost which is due to  $HO_x$  enhancements in the mesosphere above 55 km. This net ozone loss in the upper stratosphere and mesosphere is mainly due to odd hydrogen ( $HO_x$ ) catalytic destruction cycles (R14 and R15 Reactions R6 and R7) (Jackman et al., 2005) and is short-lived. Since  $HO_x$  species have a shorter lifetime, the recovery of ozone is faster. For the extreme event, after the event stops, ozone enhancements upto 25 % is observed in the mesosphere and above 80 km.

$\tilde{NO}_y$ -NO is quite long lived down at 40-60 km altitude and below so the ozone loss due to the  $NO_x$  catalytic cycle seems to be persistent. The ozone loss occurs during day time when NO reacts with ozone to form  $NO_2$ , which is then photolysed back to NO and this catalytic cycle between NO and  $NO_2$ , related to daytime continues (see reactions R20 and R21 Reactions R12 and R13). In the beginning, the amount of  $\tilde{NO}_y$  was not enough for ozone loss but at the end of the event, the accumulation is large enough for significant ozone depletion which stays on and produces a diurnal cycle between 40 km and 80 km due to  $NO_x/HO_x$  cycles as seen from the Figure-17. The continuing ozone loss in the middle and upper stratosphere, after the event stops, figure 21. The magnitude of depletion with respect to the diurnal cycle and altitude has some considerable variation. Verronen et al. (2005) used a one dimensional chemical model, Sodankylä Ion and neutral Chemistry model (SIC) for ionospheric D-region studies. They studied the effects of ion-chemistry on the neutral atmosphere and also the diurnal variation of  $NO_x/HO_x$  increases, as well as ozone depletions. This diurnal variation during a solar proton event or an energetic particle precipitation (EPP) event has been previously reported by Aikin and Smith (1999). Verronen et al. (2005) observed the diurnal cycle of  $O_x=O+O_3$  depletion between 40 and 85 km. They found substantial ozone loss at sunset of 28 October and even

greater loss at sunrise of 29 October followed by a recovery at 55–75 km during the noon and afternoon hours. The maximum depletion is reached just after sunset, with a 95% reduction in the  $O_x$  values at 78 km. During daytime on 30 October,  $O_x$  partly recovers but is again depleted during sunset. Rohen et al. (2005) also studied the Halloween SPE using SCHIAMACHY observations and considered 60°N magnetic latitude, which compares quite well to our 67.5°N geographic latitude. Since SCHIAMACHY measures only during daytime, they don't see a diurnal cycle in their results. With SCHIAMACHY, they reported a 20-30% ozone loss at 40-50 km in the Northern Hemisphere during the event and a 20-40% ozone loss, also during the event at 40-55 km observed by a photochemical model. This is related to the  $NO_x$  catalytic cycle that was long lived. Above 50 km and at higher altitudes, ozone recovery was faster after 50-60% loss during the event observed with SCHIAMACHY and the model which was due to the short lifetime of  $HO_x$  and photolytical reproduction of ozone. In our case, the continuing ozone loss at 40-55 km, related to the diurnal variation of  $NO_x$  is found to be ~~still 80-100~~ 60-80% for the extreme scenario as compared to the Halloween event which is just around 20%. At 60-80 km, 80-100% ozone loss is observed during the event and also the continuing loss due to the  $HO_x$  related diurnal cycle afterwards. Other two examples that provide valuable insights into the significant ozone variations that can occur during extreme space weather events were studied by Calisto et al. (2013) and Rodger et al. (2008). Calisto et al. (2013) investigated the potential effects of a Carrington-like solar event on ozone using a global 3D chemistry-climate model SOCOL v2.0. They found that the enhanced ionisation during the event led to substantial ozone depletion in the polar regions, particularly in the middle atmosphere. Due to the  $NO_x$  and  $HO_x$  enhancements, ozone depletion was found to be 60% in the mesosphere and 20% in the stratosphere for several weeks after the event started. They also showed total ozone decreased more than 20 DU in the northern hemisphere. Rodger et al. (2008) examined the relationship between SPEs and ozone depletion using ground-based observations and modeling. They used the Sodankylä Ion and Neutral Chemistry (SIC) model and investigated the Carrington event of August/September 1859 and found that SPEs can cause localized ozone depletion in the polar regions, primarily through the production of  $NO_x$ . The most important SPE-driven atmospheric response is an unusually strong and long-lived  $O_x$  decrease in the upper stratosphere ( $O_x$  levels drop by 40%) primarily caused by the very large fluxes of >30 MeV protons. Considering these studies, it is crucial to recognize that the ion chemistry processes during SPEs can lead to ozone changes that go beyond what is typically captured in fixed parameterizations or standard models. The enhanced ionisation and subsequent chemical reactions can influence ozone concentrations, particularly in the polar regions. Therefore, when studying the impact of SPEs on ozone, it is important to consider the effects of ion chemistry processes and their potential role in generating substantial ozone variations. By incorporating these processes into models, we can better understand the complex interplay between extreme space weather events, ion chemistry, and ozone dynamics, ultimately improving our ability to assess the impacts of such events on Earth's atmosphere.

## 5 Impact of chlorine ions on ozone loss

The evaluation of the model results with MIPAS observations gave us confidence in the model. Thus, the impact of chlorine ion-chemistry on ozone loss could be assessed using the model. According to the model, we ~~find~~ found the ozone loss in the

stratosphere and lower mesosphere during the event. Figure 18-22 shows the relative difference of the ion-chemistry model with  $O(^1D)$  in photo-chemical equilibrium including chlorine ions w.r.t. the model without chlorine ions for daytime and ~~night-time~~nighttime. The difference in this case here is calculated for daily averaged data for each day. A loss of 2.5 % during daytime at an altitude range of 40-60 km and about 10 % during ~~night-time~~nighttime, at an altitude of 50-70 km is observed during the event day. Negative chlorine species directly increase the concentrations of uncharged active chlorine compounds. Through their catalytic cycles, these uncharged chlorine compounds ~~through their catalytic cycles~~ can be responsible for ozone loss at different altitudes which is also dependent on illumination conditions. The  $ClO_x$  catalytic cycle (~~R23 and R24~~R15 and R16) is responsible for the ozone loss at 40-50 km. There is a slight difference between day-time and ~~night-time~~nighttime in the loss observed in terms of altitude range, which is expected. This difference can be explained by the difference of the diurnal cycle of ClO during daytime and nighttime. The catalytic ozone loss cycles relevant in the stratosphere-mesosphere are the ClO+O (Reactions R15, R16 and R17) and ClO+HO<sub>2</sub> (Reactions R18, R21 and R19) that also need solar light, since O is formed by photolysis. During daytime, ClO photolyses in the mesosphere but not in the stratosphere, so ClO is not observed in the mesosphere. The ClO+HO<sub>2</sub> cycle produces HOCl which also photolyses during daytime producing Cl through Reaction R20. So during daytime, Cl is more important than ClO. But during nighttime, ClO accumulates in the mesosphere and in the stratosphere, it is mainly ClONO<sub>2</sub> due to Reaction R32. As we see from our results, during the event day on October 28 and also on October 29, the ClO mixing ratios were found to be higher for night-time around 60-70 km compared to daytime.

Hence, the ozone loss occurs more in the upper stratosphere-mesosphere around 50-70 km for nighttime, thereby producing the difference of the ozone loss in the altitude range. Loss of 0.6% during day-time and 2% during ~~night-time~~nighttime is observed in the altitude range of 30-40 km, ~~for which the~~. The  $ClO_x$  cycles with Reactions R31, R32, R33 and Reactions R35, R36, R37 and R38 are responsible R28, R29, R30 and Reactions R32, R33, R34 and R35 are responsible at this altitude range for both daytime and nighttime. Furthermore, a continuous ozone formation of 2% both during daytime and ~~night-time~~around nighttime is observed. This increase is linked to enhanced atomic oxygen production by O<sub>2</sub> photolysis in solar maximum conditions (Marsh et al., 2007). It is observed at an altitude range of 60-70 km is observed after the event stops which is also due to the impact of chlorine ion-chemistry km for daytime and 50-70 km for nighttime.

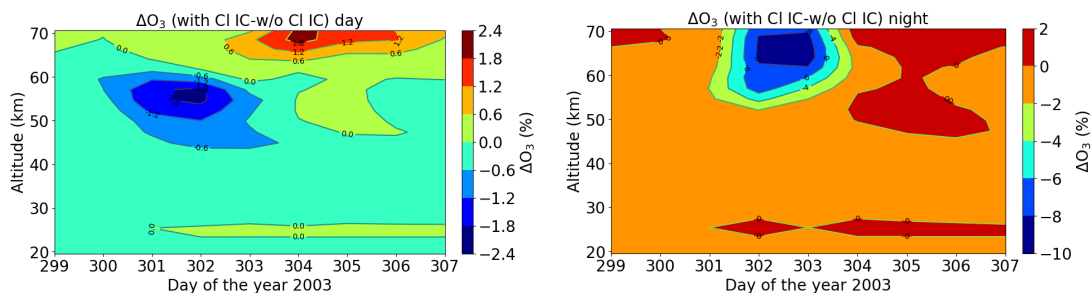


**Figure 22.** Relative difference of the model with full ion-chemistry and  $O(^1D)$  in photo-chemical equilibrium including chlorine ions w.r.t. the model without chlorine ion-chemistry for the Halloween SPE: daytime (left) and ~~night-time~~nighttime (right). The difference here is calculated for daily averaged data.

Figure 19-23 shows the relative differences of the model setting with ion-chemistry and  $O(^1D)$  in photo-chemical equilibrium w.r.t. the model setting without chlorine ion-chemistry comparing the Halloween SPE and the extreme event in order to assess the impact of chlorine ion-chemistry on ozone loss during the event day. A very small impact of the chlorine ions around 10-20% is observed on the event day. Qualitatively, it was a bit more for the extreme event compared to the Halloween SPE, which that could be more important for higher forcing. An increase of around 5% for ozone is also seen after the event stops for the extreme scenario. The extreme run doesn't show any impact of chlorine ion-chemistry on ozone loss at 70-75 km while the Halloween SPE does. This can be explained by the ClO and HOCl responses to SPEs and due to the  $ClO_x$  catalytic cycle. At an altitude of 70-75 km, ClO decrease for the sensitivity runs for both ion-chemistry with  $O(^1D)$  in photo-chemical equilibrium and without chlorine ions is larger for the extreme event compared to the Halloween SPE (figure 16). This is one contributing factor as to why we don't see an impact on ozone loss at these altitudes. Kalakoski et al. (2020) used WACCM-D to investigate ozone depletion around 50-60 km after the onset of the SPE as explained in Sect. 4. They studied the effect in both the hemispheres and the duration and altitude range of this extra ozone loss correspond to  $NO_x$  and enhanced  $Cl_x (=Cl+ClO)$  mixing ratios. An ozone loss of 0.2 ppm in both the hemispheres was observed after the event. Around 70 km, the ozone loss was due to short lived  $HO_x$ . And around 50 km, it is driven by  $NO_x$  and  $Cl_x$  that lasts longer with maximum ozone decrease seen about 30 days after the event onset. Since HCl response to SPEs is partly due to chlorine ion-chemistry which converts it to Cl, ClO and HOCl (Winkler et al., 2009), this is also indirectly an effect of the chlorine ion-chemistry. They also see an increase in ozone, around 0.2 ppm throughout the period near the secondary ozone maximum above 80 km, which is also due to  $O_2$  photolysis as discussed above. We observe a continuous increase of  $O_3$  after the event, which is about 5%. This increase was seen around 50-60 km for the Halloween SPE and 50-75 km for the extreme scenario.

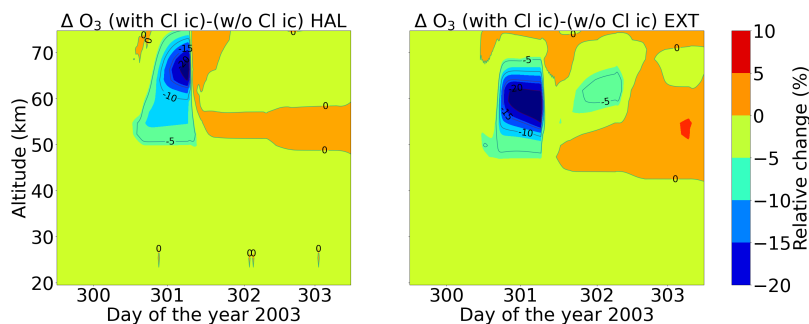


**Figure 23.** Relative difference of the model simulations: full ion-chemistry with  $O(^1D)$  in photo-chemical equilibrium and with chlorine ions w.r.t. the model setting without chlorine ion-chemistry comparing the Halloween SPE (left) and extreme scenario (right). The data shown here is not daily averaged but the real model time step.

## 6 Discussions and conclusions

Using satellite data (MIPAS on ENVISAT), the state of the art 1D ion-chemistry ExoTIC model has been validated. Two event classes were modelled and chlorine ion-chemistry and its impact on ozone has been evaluated. ExoTIC has been used to study

710 the short-term constituent changes caused by the Halloween SPE of 2003. The results demonstrated here show a comparison  
of stratospheric and mesospheric composition changes observed by MIPAS in the polar cap region with simulations performed  
by ExoTIC. The inter-comparison of the model and MIPAS observations allowed for an evaluation of the overall ability of the  
ExoTIC model to reproduce observed atmospheric perturbations generated by solar proton events, particularly with respect to  
changes in the chlorine species, SPE induced  $\text{NO}_y$  enhancements and ozone depletion. Polar upper stratospheric and lower  
715 mesospheric  $\text{NO}_y$  increased by over 40 ppbv and mesospheric ozone decreased by over 70 % during the SPE period. The  
inter-comparison also tested and identified deficiencies in the chemical schemes, particularly with respect to nitrogen and  
chlorine chemistry which is relevant for stratospheric ozone. Short-time enhancements of HOCl and ClONO<sub>2</sub> were observed  
by MIPAS and also reproduced in the simulations with different model settings. Application of MIPAS averaging kernels to the  
ExoTIC output made the inter-comparison much better. HOCl enhancements were reproduced best for the model simulation  
720 with ~~full~~ ion-chemistry where O(<sup>1</sup>D) was set to photo-chemical equilibrium. An HOCl enhancement of more than 0.2 ppbv  
occurred roughly during the event as observed by MIPAS. The HOCl enhancements with averaging kernels as found in ExoTIC  
and its temporal variation agree quite well with MIPAS. The ozone depletion simulated by the model extends over a large  
altitude range as compared to MIPAS observations. Jackman et al. (2008) found the opposite from WACCM3 results in the  
northern hemisphere in terms of altitude range. The encountered differences between the model and observations for ClONO<sub>2</sub>  
725 enhancements, it's underestimation by the model are related to a smaller availability of ClO in the polar region before the SPE.  
The ClONO<sub>2</sub> peak is observed at the same altitude for both the model and MIPAS, but the enhancements in MIPAS is observed  
earlier and the peak values seem to agree quite well even without the averaging kernels applied. Jackman et al. (2008) also  
found the ClONO<sub>2</sub> peak at the same altitude with WACCM3 but the values were underestimated by a factor of two compared  
to MIPAS.

730 The comparison of the Halloween SPE and the extreme solar event of 775 A.D. showed long lasting stratospheric ozone  
loss for the extreme scenario. A long lasting impact was also found for the chlorine species like HOCl and HCl in case of the  
extreme scenario. Loss of HCl was underestimated by the parameterised model which was also found by Winkler et al. (2009)  
during the solar proton event in July 2000 in the northern polar region. For the extreme event, the parameterised model showed  
much higher  $\text{NO}_y$  enhancements, about a 1000 ppm in the mesosphere and lower thermosphere. HO<sub>x</sub> enhancements of 0.1  
735 ppm was found during the extreme event which went further down in altitude upto 40 km, for all the model case studies. An  
impact of around 10-20 % on ozone loss was found due to the chlorine ions for the two events, a bit stronger for the extreme  
scenario ~~-, which that~~ is more important for higher forcing. Ozone formation was observed after the event which is also due  
to the impact of chlorine ion-chemistry. For the Halloween event with temporal ionisation rates, ozone loss of 2.4 % during  
day-time and 10 % during ~~night-time~~ nighttime was observed during the event that is ~~due to~~ also due to the included chlorine  
740 ion-chemistry. Ozone formation of 2-4 % was ~~also~~ found after the event both during day-time and ~~night-time~~ nighttime.

In general, ExoTIC simulations reproduced the impacts of the Halloween SPE quite well, mainly for HOCl and  $\text{NO}_y$ .  
However, the initial state of the atmosphere in the simulations could be an important factor for some variability in the model  
results and MIPAS observations. Future work will focus on including the D-region ion-chemistry into the global 3D chemistry  
climate model EMAC (ECHAM/MESSy) and the evaluation of the chemistry with MIPAS observations in a setup considering

745 atmospheric dynamics. While previous results with UBIC focused on the solar proton event in July 2000 in the northern polar region and compared to the HCl measurements from Halogen Occultation Experiment instrument (HALOE), we compare with MIPAS observations. Since MIPAS observations provide a better picture of the polar cap region as compared to HALOE observations that are less densely sampled, these results suggest that the validated D-region ion-chemistry setup in the ExoTIC model can be trusted to implement in a global 3D model. The problem of O(<sup>1</sup>D) in the ion-chemistry in ExoTIC should be taken  
750 into account which was however related to the neutral chemistry model as explained in Sect. 2.2.1. For a global 3D chemistry climate model, at least in EMAC (ECHAM/MESSy), that we are considering for the implementation, the ion-chemistry is part of the normal chemistry solver and in that case, the O(<sup>1</sup>D) formation rate should be not too large and it should work without doing anything to O(<sup>1</sup>D). This setup will be first evaluated with MIPAS observations and since EMAC can already provide the data at the MIPAS footprints, the modelled data can be sampled at MIPAS measurement local times. The model will then  
755 considered for experiments in different setups to look at the dynamical impacts with and without the D-region ion-chemistry with important chemical reactions involving water, chlorine and NO<sup>+</sup> cluster ions.

## Appendix A: Chlorine Ions and Ionic Reactions

In this Appendix, the reactions involving the chlorine ions and their rate coefficients used in ExoTIC is listed.

**Table A1.** T is the temperature in K, and M is the total air density in  $\text{cm}^{-3}$

Reactants	Products	Rate coefficient	Source
$\text{Cl}^- + \text{Cl}_2$	$\text{Cl}_3^-$	$9 \times 10^{-30} \times (\text{M})$	Amelynck et al. (1994)
$\text{Cl}^- + \text{CO}_2$	$\text{Cl}^-(\text{CO}_2)$	$6 \times 10^{-29} \times \left(\frac{300}{\text{T}}\right)^2 \times (\text{M})$	Kopp and Fritzenwallner (1997)
$\text{Cl}^- + \text{H}_2\text{O}$	$\text{Cl}^-(\text{H}_2\text{O})$	$2 \times 10^{-29} \times \left(\frac{300}{\text{T}}\right)^2 \times (\text{M})$	Turco (1977)
$\text{Cl}^- + \text{HCl}$	$\text{Cl}^-(\text{HCl})$	$1 \times 10^{-27} \times (\text{M})$	Kazil et al. (2003)
$\text{Cl}^-(\text{CO}_2)$	$\text{Cl}^- + \text{CO}_2$	$2.6 \times 10^{-5} \times \left(\frac{300}{\text{T}}\right)^3 \times e^{-\frac{4000}{\text{T}}} \times (\text{M})$	Kopp and Fritzenwallner (1997)
$\text{Cl}^-(\text{H}_2\text{O})$	$\text{Cl}^- + \text{H}_2\text{O}$	$9.2 \times 10^{-5} \times \left(\frac{300}{\text{T}}\right)^3 \times e^{-\frac{7450}{\text{T}}} \times (\text{M})$	Kopp and Fritzenwallner (1997)
$\text{Cl}^-(\text{HCl})$	$\text{Cl}^- + \text{HCl}$	$3.33 \times 10^{-5} \times \left(\frac{300}{\text{T}}\right) \times e^{-\frac{11926}{\text{T}}} \times (\text{M})$	Kopp and Fritzenwallner (1997)
$\text{NO}_3^- + \text{HCl}$	$\text{NO}_3^-(\text{HCl})$	$5.22 \times 10^{-28} \times \left(\frac{300}{\text{T}}\right)^{2.62}$	Kopp and Fritzenwallner (1997)
$\text{OH}^- + \text{HCl}$	$\text{Cl}^- + \text{H}_2\text{O}$	$1.5 \times 10^{-9} \times \left(\frac{300}{\text{T}}\right)^5$	Kopp and Fritzenwallner (1997)
$\text{Cl}^- + \text{ClONO}_2$	$\text{NO}_3^- + \text{Cl}_2$	$9.2 \times 10^{-10}$	Turco (1977)
$\text{Cl}^- + \text{HNO}_3$	$\text{NO}_3^- + \text{HCl}$	$2.8 \times 10^{-9}$	Huey (1996)
$\text{Cl}^- + \text{H}$	$\text{e} + \text{HCl}$	$9.6 \times 10^{-10}$	Turco (1977)
$\text{Cl}^- + \text{N}_2\text{O}_5$	$\text{NO}_3^- + \text{ClNO}_2$	$9.4 \times 10^{-10}$	Amelynck et al. (1994)
$\text{Cl}^-(\text{H}_2\text{O}) + \text{Cl}_2$	$\text{Cl}_3^- + \text{H}_2$	$1.09 \times 10^{-9}$	Kopp and Fritzenwallner (1997)
$\text{Cl}^-(\text{H}_2\text{O}) + \text{HCl}$	$\text{Cl}^-(\text{HCl}) + \text{H}_2\text{O}$	$1.30 \times 10^{-9}$	Kopp and Fritzenwallner (1997)
$\text{Cl}^-(\text{H}_2\text{O}) + \text{HNO}_3$	$\text{NO}_3^-(\text{HCl}) + \text{H}_2\text{O}$	$2.85 \times 10^{-9}$	Kopp and Fritzenwallner (1997)
$\text{Cl}^-(\text{H}_2\text{O}) + \text{H}$	$\text{e} + \text{H}_2\text{O} + \text{HCl}$	$8 \times 10^{-11}$	Kopp and Fritzenwallner (1997)
$\text{Cl}^-(\text{HCl}) + \text{Cl}_2$	$\text{Cl}_3^- + \text{HCl}$	$5.3 \times 10^{-10}$	Kopp and Fritzenwallner (1997)
$\text{Cl}^-(\text{HCl}) + \text{HNO}_3$	$\text{NO}_3^-(\text{HCl}) + \text{HCl}$	$2.48 \times 10^9$	Kopp and Fritzenwallner (1997)
$\text{Cl}^- + \text{NO}_2$	$\text{NO}_2^- + \text{Cl}$	$6.0 \times 10^{-12}$	Kopp and Fritzenwallner (1997)
$\text{Cl}^- + \text{O}_3$	$\text{ClO}^- + \text{O}_2$	$5.0 \times 10^{-13}$	Turco (1977)
$\text{Cl}_2^- + \text{HNO}_3$	$\text{NO}_3^-(\text{HCl}) + \text{Cl}$	$4.8 \times 10^{-10}$	Amelynck et al. (1994)
$\text{Cl}_2^- + \text{NO}_2$	$\text{Cl}^- + \text{ClNO}_2$	$4.0 \times 10^{-11}$	Kopp and Fritzenwallner (1997)
$\text{Cl}_2^- + \text{O}_3$	$\text{O}_3^- + \text{Cl}_2$	$2.0 \times 10^{-12}$	Kopp and Fritzenwallner (1997)
$\text{Cl}_3^- + \text{HNO}_3$	$\text{NO}_3^-(\text{HCl}) + \text{Cl}_2$	$1.3 \times 10^{-9}$	Amelynck et al. (1994)
$\text{CO}_3^- + \text{ClONO}_2$	$\text{NO}_3^- + \text{ClO} + \text{CO}_2$	$2.1 \times 10^{-9}$	Kopp and Fritzenwallner (1997)
$\text{CO}_3^- + \text{HCl}$	$\text{Cl}^- + \text{OH} + \text{CO}_2$	$3.0 \times 10^{-11}$	Kopp and Fritzenwallner (1997)
$\text{CO}_4^- + \text{HCl}$	$\text{Cl}^-(\text{HO}_2) + \text{CO}_2$	$1.2 \times 10^{-11}$	Kopp and Fritzenwallner (1997)

continued



Reactants	Products	Rate coefficient	Source
$\text{NO}_2^- + \text{Cl}_2$	$\text{Cl}_2^- + \text{NO}_2$	$6.8 \times 10^{-10}$	Kopp and Fritzenwallner (1997)
$\text{NO}_2^- + \text{HCl}$	$\text{Cl}^- + \text{HNO}_2$	$1.4 \times 10^{-9}$	Kopp and Fritzenwallner (1997)
$\text{NO}_3^- + \text{HCl}$	$\text{Cl}^- + \text{HNO}_2$	$1.0 \times 10^{-12}$	Kopp and Fritzenwallner (1997)
$\text{NO}_3^- (\text{HCl}) + \text{HNO}_3$	$\text{NO}_3^- (\text{HNO}_3) + \text{HCl}$	$7.6 \times 10^{-10}$	Amelynck et al. (1994)
$\text{O}^- + \text{HCl}$	$\text{Cl}^- + \text{OH}$	$2.0 \times 10^{-9}$	Turco (1977)
$\text{O}_2^- + \text{HCl}$	$\text{Cl}^- + \text{HO}_2$	$1.6 \times 10^{-9}$	Turco (1977)
$\text{O}_3^- + \text{Cl}_2$	$\text{Cl}^- + \text{ClO} + \text{O}_2$	$1.3 \times 10^{-9}$	Turco (1977)
$\text{ClO}^- + \text{NO}$	$\text{Cl}^- + \text{NO}_2$	$2.9 \times 10^{-11} \times 0.5$	Turco (1977)
$\text{ClO}^- + \text{O}_3$	$\text{Cl}^- + \text{O}_2 + \text{O}_2$	$6.0 \times 10^{-11}$	Turco (1977)
$\text{ClO}^- + \text{O}_3$	$\text{ClO} + \text{O}_3^-$	$1.0 \times 10^{-11}$	Turco (1977)
$\text{O}^- + \text{Cl}$	$\text{Cl}^- + \text{O}$	$1.0 \times 10^{-10}$	Turco (1977)
$\text{O}^- + \text{ClO}$	$\text{Cl}^- + \text{O}_2$	$1.0 \times 10^{-10}$	Turco (1977)
$\text{O}_2^- + \text{Cl}$	$\text{Cl}^- + \text{O}_2$	$1.0 \times 10^{-10}$	Turco (1977)
$\text{O}_2^- + \text{ClO}$	$\text{ClO}^- + \text{O}_2$	$1.0 \times 10^{-10}$	Turco (1977)
$\text{OH}^- + \text{Cl}$	$\text{Cl}^- + \text{OH}$	$1.0 \times 10^{-10}$	Turco (1977)
$\text{OH}^- + \text{ClO}$	$\text{ClO}^- + \text{OH}$	$1.0 \times 10^{-10}$	Turco (1977)
$\text{CO}_3^- + \text{Cl}$	$\text{Cl}^- + \text{O} + \text{CO}_2$	$1.0 \times 10^{-10}$	Turco (1977)
$\text{CO}_3^- + \text{Cl}$	$\text{ClO}^- + \text{CO}_2$	$1.0 \times 10^{-10}$	Turco (1977)
$\text{CO}_3^- + \text{ClO}$	$\text{Cl}^- + \text{CO}_2 + \text{O}_2$	$1.0 \times 10^{-10}$	Turco (1977)
$\text{CO}_4^- + \text{Cl}$	$\text{Cl}^- + \text{O}_2 + \text{CO}_2$	$1.0 \times 10^{-10}$	Turco (1977)
$\text{CO}_4^- + \text{ClO}$	$\text{ClO}^- + \text{O}_2 + \text{CO}_2$	$1.0 \times 10^{-10}$	Turco (1977)
$\text{NO}_2^- + \text{Cl}$	$\text{Cl}^- + \text{NO}_2$	$1.0 \times 10^{-10}$	Turco (1977)
$\text{NO}_2^- + \text{ClO}$	$\text{Cl}^- + \text{NO}_3$	$1.0 \times 10^{-10}$	Turco (1977)
$\text{HCO}_3^- + \text{Cl}$	$\text{Cl}^- + \text{OH} + \text{CO}_2$	$1.0 \times 10^{-10}$	Turco (1977)
$\text{HCO}_3^- + \text{ClO}$	$\text{Cl}^- + \text{HO}_2 + \text{CO}_2$	$1.0 \times 10^{-10}$	Turco (1977)
$\text{ClO}^- + \text{O}$	$\text{Cl}^- + \text{O}_2$	$2.0 \times 10^{-10}$	Turco (1977)
$\text{H}^+ + \text{Cl}^-$	$\text{Cl}$	$6 \times 10^{-8} \times \left(\frac{300}{T}\right)^{0.5} + 1.25 \times 10^{-25} \times \left(\frac{300}{T}\right)^4 \times (\text{M})^*$	Arijs et al. (1987)
$\text{H}^+ + \text{Cl}_2^-$	$\text{Cl}_2$		
$\text{H}^+ + \text{Cl}_3^-$	$\text{Cl}_2 + \text{Cl}$		
$\text{H}^+ + \text{Cl}^- (\text{HCl})$	$\text{Cl} + \text{HCl}$		
$\text{H}^+ + \text{Cl}^- (\text{H}_2\text{O})$	$\text{Cl} + \text{H}_2\text{O}$		

\* The coefficient is the same for all the reactions below

Reactants	Products	Rate coefficient	Source
$H^+ + Cl^-(CO_2)$	$Cl + CO_2$		
$H^+ + Cl^-(HO_2)$	$Cl + HO_2$		
$H^+ + ClO^-$	$ClO$		

760 *Code availability.* The Exoplanetary Terrestrial Ion Chemistry (EXoTIC) is continuously developed and applied in the group 'Middle Atmosphere Solar Variability and Climate Interactions (MSK)' at IMK-ASF. The exact code version used to produce the simulation results can be made available upon request from Miriam Sinnhuber (miriam.sinnhuber@kit.edu).

*Data availability.* ~~MIPAS data are available from <https://www.imk-asf.kit.edu/english/308.php> (Institute of Meteorology and Climate Research, 2022) after registration.~~ The "raw" MIPAS V5H data set, i.e. ClONO<sub>2</sub>, HNO<sub>3</sub>, HOCl, N<sub>2</sub>O<sub>5</sub>, NO, NO<sub>2</sub>, and O<sub>3</sub> vertical profiles and corresponding averaging kernel matrices for October and November 2003 is available on doi: 10.5445/IR/1000156935.

765 *Author contributions.* MB and MS discussed the ideas. MB wrote the paper. MB and MS worked on the code and simulation results for the ExoTIC ion-chemistry model. MB worked on the visualisation and analysis of the MIPAS data and AL helped with the MIPAS averaging kernels. TC, GS and BF provided access to MIPAS data and helped with technical questions regarding the correct use of MIPAS data. JW and OY developed AISstorm and provided us with the ionisation rates. IU calculated the ionisation rates for the extreme solar event of 775 A.D. All authors contributed to reviewing and editing the manuscript.

770 *Competing interests.* At least one of the co-authors is a member of the editorial board of Atmospheric Chemistry and Physics.

*Acknowledgements.* This research has been supported by the German Research Foundation (DFG) under the project SI 1088/7-1. The AISstorm model is funded by the German Science Foundation (DFG project WI4417/2-1). J.M. Wissing also thanks to support from the German Aerospace Center (DLR). The authors acknowledge the NOAA National Centers for Environmental Information (<https://ngdc.noaa.gov/stp/satellite/poes/dataaccess.html>) for the POES and Metop particle data used in this study.

- Aikin, A. C. and Smith, H. J. P.: Mesospheric constituent variations during electron precipitation events, , 104, 26,457–26,471, <https://doi.org/10.1029/1999JD900752>, 1999.
- Amelynck, C., Fussen, D., and Arijs, E.: Reactions of nitric acid with di- and trichloride ions, di- and tri-iodide ions and with CO-4 in the gas phase, *International Journal of Mass Spectrometry and Ion Processes*, 133, 13–28, [https://doi.org/https://doi.org/10.1016/0168-1176\(94\)03950-X](https://doi.org/https://doi.org/10.1016/0168-1176(94)03950-X), 1994.
- Andersson, M. E., Verronen, P. T., Marsh, D. R., Päivärinta, S.-M., and Plane, J. M. C.: WACCM-D—Improved modeling of nitric acid and active chlorine during energetic particle precipitation, *Journal of Geophysical Research: Atmospheres*, 121, 10,328–10,341, <https://doi.org/https://doi.org/10.1002/2015JD024173>, 2016.
- Arijs, E., Nevejans, D., and Ingels, J.: Stratospheric positive ion composition measurements and acetonitrile detection: a consistent picture?, *International Journal of Mass Spectrometry and Ion Processes*, 81, 15–31, [https://doi.org/https://doi.org/10.1016/0168-1176\(87\)80003-4](https://doi.org/https://doi.org/10.1016/0168-1176(87)80003-4), 1987.
- Barth, C. A.: Nitric oxide in the lower thermosphere, *Planetary and Space Science*, 40, 315–336, [https://doi.org/https://doi.org/10.1016/0032-0633\(92\)90067-X](https://doi.org/https://doi.org/10.1016/0032-0633(92)90067-X), 1992.
- Bates, D. R. and Nicolet, M.: The photochemistry of atmospheric water vapor, *Journal of Geophysical Research (1896-1977)*, 55, 301–327, <https://doi.org/https://doi.org/10.1029/JZ055i003p00301>, 1950.
- Calisto, M., Usoskin, I., and Rozanov, E.: Influence of a Carrington-like event on the atmospheric chemistry, temperature and dynamics: revised, *Environmental Research Letters*, 8, 045 010, <https://doi.org/10.1088/1748-9326/8/4/045010>, 2013.
- Chakrabarty, D. and Ganguly, S.: On significant quantities of negative ions observed around the mesopause, *Journal of Atmospheric and Terrestrial Physics*, 51, 983–989, [https://doi.org/https://doi.org/10.1016/0021-9169\(89\)90013-5](https://doi.org/https://doi.org/10.1016/0021-9169(89)90013-5), 1989.
- Chipperfield, M. P.: Multiannual simulations with a three-dimensional chemical transport model, *Journal of Geophysical Research: Atmospheres*, 104, 1781–1805, <https://doi.org/https://doi.org/10.1029/98JD02597>, 1999.
- Cliver, E. W., Schrijver, C. J., Shibata, K., and Usoskin, I. G.: Extreme solar events, *Living Reviews in Solar Physics*, 19, <https://doi.org/10.1007/s41116-022-00033-8>, 2022.
- Connor, B. J., Siskind, D. E., Tsou, J. J., Parrish, A., and Remsberg, E. E.: Ground-based microwave observations of ozone in the upper stratosphere and mesosphere, , 99, 16,757–16,770, <https://doi.org/10.1029/94JD01153>, 1994.
- Damiani, A., Funke, B., Marsh, D. R., López-Puertas, M., Santee, M. L., Froidevaux, L., Wang, S., Jackman, C. H., von Clarmann, T., Gardini, A., Cordero, R. R., and Storini, M.: Impact of January 2005 solar proton events on chlorine species, *Atmospheric Chemistry and Physics*, 12, 4159–4179, <https://doi.org/10.5194/acp-12-4159-2012>, 2012.
- Daniel, J. S., Solomon, S., Portmann, R. W., and Garcia, R. R.: Stratospheric ozone destruction: The importance of bromine relative to chlorine, *Journal of Geophysical Research: Atmospheres*, 104, 23 871–23 880, <https://doi.org/https://doi.org/10.1029/1999JD900381>, 1999.
- Fischer, H., Birk, M., Blom, C., Carli, B., Carlotti, M., von Clarmann, T., Delbouille, L., Dudhia, A., Ehhalt, D., Endemann, M., Flaud, J. M., Gessner, R., Kleinert, A., Koopman, R., Langen, J., López-Puertas, M., Mosner, P., Nett, H., Oelhaf, H., Perron, G., Remedios, J., Ridolfi, M., Stiller, G., and Zander, R.: MIPAS: an instrument for atmospheric and climate research, *Atmospheric Chemistry and Physics*, 8, 2151–2188, <https://doi.org/10.5194/acp-8-2151-2008>, 2008.

- 810 Fritzenwallner, J. and Kopp, E.: Model calculations of the negative ion chemistry in the mesosphere with special emphasis on the chlorine species and the formation of cluster ions, *Advances in Space Research*, 21, 891–894, [https://doi.org/https://doi.org/10.1016/S0273-1177\(97\)00649-2](https://doi.org/https://doi.org/10.1016/S0273-1177(97)00649-2), proceedings of the C0.1 Symposium of COSPAR Scientific Commission C, 1998.
- Funke, B., López-Puertas, M., von Clarmann, T., Stiller, G. P., Fischer, H., Glatthor, N., Grabowski, U., Höpfner, M., Kellmann, S., Kiefer, M., Linden, A., Mengistu Tsidu, G., Milz, M., Steck, T., and Wang, D. Y.: Retrieval of stratospheric NO<sub>x</sub> from 5.3 and 6.2  $\mu\text{m}$  nonlocal  
815 thermodynamic equilibrium emissions measured by Michelson Interferometer for Passive Atmospheric Sounding (MIPAS) on Envisat, *Journal of Geophysical Research: Atmospheres*, 110, <https://doi.org/https://doi.org/10.1029/2004JD005225>, 2005.
- Funke, B., Baumgaertner, A., Calisto, M., Egorova, T., Jackman, C. H., Kieser, J., Krivolutsky, A., López-Puertas, M., Marsh, D. R., Reddmann, T., Rozanov, E., Salmi, S.-M., Sinnhuber, M., Stiller, G. P., Verronen, P. T., Versick, S., von Clarmann, T., Vyushkova, T. Y., Wieters, N., and Wissing, J. M.: Composition changes after the "Halloween" solar proton event: the High Energy Particle Precipitation  
820 in the Atmosphere (HEPPA) model versus MIPAS data intercomparison study, *Atmospheric Chemistry and Physics*, 11, 9089–9139, <https://doi.org/10.5194/acp-11-9089-2011>, 2011.
- Glatthor, N., von Clarmann, T., Fischer, H., Funke, B., Gil-López, S., Grabowski, U., Höpfner, M., Kellmann, S., Linden, A., López-Puertas, M., Mengistu Tsidu, G., Milz, M., Steck, T., Stiller, G. P., and Wang, D.-Y.: Retrieval of stratospheric ozone profiles from MIPAS/ENVISAT limb emission spectra: a sensitivity study, *Atmospheric Chemistry and Physics*, 6, 2767–2781, <https://doi.org/10.5194/acp-6-2767-2006>, 2006.  
825
- Harvey, V. L., Randall, C. E., and Collins, R. L.: Chemical definition of the mesospheric polar vortex, *Journal of Geophysical Research: Atmospheres*, 120, 10,166–10,179, <https://doi.org/https://doi.org/10.1002/2015JD023488>, 2015.
- Herbst, K., Grenfell, J. L., Sinnhuber, M., and Wunderlich, F.: INCREASE: An updated model suite to study the Influence of Cosmic Rays on Exoplanetary Atmospheres, *Astronomische Nachrichten*, 343, e210 072, <https://doi.org/https://doi.org/10.1002/asna.20210072>, 2022.
- 830 Herbst, Konstantin, Grenfell, John Lee, Sinnhuber, Miriam, Rauer, Heike, Heber, Bernd, Banjac, Sasa, Scheucher, Markus, Schmidt, Vanessa, Gebauer, Stefanie, Lehmann, Ralph, and Schreier, Franz: A new model suite to determine the influence of cosmic rays on (exo)planetary atmospheric biosignatures - Validation based on modern Earth, *A&A*, 631, A101, <https://doi.org/10.1051/0004-6361/201935888>, 2019.
- Höpfner, M., von Clarmann, T., Fischer, H., Funke, B., Glatthor, N., Grabowski, U., Kellmann, S., Kiefer, M., Linden, A., Milz, M., Steck, T., Stiller, G. P., Bernath, P., Blom, C. E., Blumenstock, T., Boone, C., Chance, K., Coffey, M. T., Friedl-Vallon, F., Griffith, D., Hannigan, J. W., Hase, F., Jones, N., Jucks, K. W., Keim, C., Kleinert, A., Kouker, W., Liu, G. Y., Mahieu, E., Mellqvist, J., Mikuteit, S.,  
835 Notholt, J., Oelhaf, H., Piesch, C., Reddmann, T., Ruhnke, R., Schneider, M., Strandberg, A., Toon, G., Walker, K. A., Warneke, T., Wetzels, G., Wood, S., and Zander, R.: Validation of MIPAS ClONO<sub>2</sub> measurements, *Atmospheric Chemistry and Physics*, 7, 257–281, <https://doi.org/10.5194/acp-7-257-2007>, 2007a.
- Höpfner, M., von Clarmann, T., Fischer, H., Funke, B., Glatthor, N., Grabowski, U., Kellmann, S., Kiefer, M., Linden, A., Milz, M., Steck, T., Stiller, G. P., Bernath, P., Blom, C. E., Blumenstock, T., Boone, C., Chance, K., Coffey, M. T., Friedl-Vallon, F., Griffith, D., Hannigan, J. W., Hase, F., Jones, N., Jucks, K. W., Keim, C., Kleinert, A., Kouker, W., Liu, G. Y., Mahieu, E., Mellqvist, J., Mikuteit, S.,  
840 Notholt, J., Oelhaf, H., Piesch, C., Reddmann, T., Ruhnke, R., Schneider, M., Strandberg, A., Toon, G., Walker, K. A., Warneke, T., Wetzels, G., Wood, S., and Zander, R.: Validation of MIPAS ClONO<sub>2</sub> measurements, *Atmospheric Chemistry and Physics*, 7, 257–281, <https://doi.org/10.5194/acp-7-257-2007>, 2007b.
- 845 Huey, L.: The kinetics of the reactions of Cl-, O-, and O2- with HNO<sub>3</sub>: Implications for measurement of HNO<sub>3</sub> in the atmosphere, *International Journal of Mass Spectrometry and Ion Processes*, 153, 145–150, [https://doi.org/https://doi.org/10.1016/0168-1176\(95\)04354-3](https://doi.org/https://doi.org/10.1016/0168-1176(95)04354-3), 1996.

- J. C. Farman, B. G. G. and Shanklin, J. D.: Large losses of total ozone in Antarctica reveal seasonal ClO<sub>x</sub>/NO<sub>x</sub> interaction, *Nature*, 315, 207–210, <https://doi.org/10.1038/315207a0>, 1985.
- 850 Jackman, C. H., Fleming, E. L., and Vitt, F. M.: Influence of extremely large solar proton events in a changing stratosphere, *Journal of Geophysical Research: Atmospheres*, 105, 11 659–11 670, <https://doi.org/https://doi.org/10.1029/2000JD900010>, 2000.
- Jackman, C. H., DeLand, M. T., Labow, G. J., Fleming, E. L., Weisenstein, D. K., Ko, M. K., Sinnhuber, M., and Russell, J. M.: Neutral atmospheric influences of the solar proton events in October–November 2003, *Journal of Geophysical Research: Space Physics*, 110, 2005.
- 855 Jackman, C. H., Marsh, D. R., Vitt, F. M., Garcia, R. R., Fleming, E. L., Labow, G. J., Randall, C. E., López-Puertas, M., Funke, B., von Clarman, T., and Stiller, G. P.: Short- and medium-term atmospheric constituent effects of very large solar proton events, *Atmospheric Chemistry and Physics*, 8, 765–785, <https://doi.org/10.5194/acp-8-765-2008>, 2008.
- Jones, R. and Rees, M.: Time dependent studies of the aurora—I. Ion density and composition, *Planetary and Space Science*, 21, 537–557, [https://doi.org/https://doi.org/10.1016/0032-0633\(73\)90069-X](https://doi.org/https://doi.org/10.1016/0032-0633(73)90069-X), 1973.
- 860 Kalakoski, N., Verronen, P. T., Seppälä, A., Szeląg, M. E., Kero, A., and Marsh, D. R.: Statistical response of middle atmosphere composition to solar proton events in WACCM-D simulations: the importance of lower ionospheric chemistry, *Atmospheric Chemistry and Physics*, 20, 8923–8938, <https://doi.org/10.5194/acp-20-8923-2020>, 2020.
- Kazil, J., Kopp, E., Chabrillat, S., and Bishop, J.: The University of Bern Atmospheric Ion Model: Time-dependent modeling of the ions in the mesosphere and lower thermosphere, *Journal of Geophysical Research: Atmospheres*, 108, <https://doi.org/https://doi.org/10.1029/2002JD003024>, 2003.
- 865 Kopp, E. and Fritzenwallner, J.: Chlorine and bromine ions in the D-region, *Advances in Space Research*, 20, 2111–2115, [https://doi.org/https://doi.org/10.1016/S0273-1177\(97\)00603-0](https://doi.org/https://doi.org/10.1016/S0273-1177(97)00603-0), middle Atmosphere: Changes and Electrodynamics, 1997.
- Kvissel, O.-K., Orsolini, Y. J., Stordal, F., Isaksen, I. S. A., and Santee, M. L.: Formation of stratospheric nitric acid by a hydrated ion cluster reaction: Implications for the effect of energetic particle precipitation on the middle atmosphere, *Journal of Geophysical Research: Atmospheres*, 117, <https://doi.org/https://doi.org/10.1029/2011JD017257>, 2012.
- 870 Lary, D. J.: Catalytic destruction of stratospheric ozone, *Journal of Geophysical Research: Atmospheres*, 102, 21 515–21 526, <https://doi.org/https://doi.org/10.1029/97JD00912>, 1997.
- López-Puertas, M., Funke, B., Gil-López, S., von Clarman, T., Stiller, G. P., Höpfner, M., Kellmann, S., Fischer, H., and Jackman, C. H.: Observation of NO<sub>x</sub> enhancement and ozone depletion in the Northern and Southern Hemispheres after the October–November 2003 solar proton events, *Journal of Geophysical Research: Space Physics*, 110, <https://doi.org/https://doi.org/10.1029/2005JA011050>, 2005.
- 875 Marsh, D. R., Garcia, R. R., Kinnison, D. E., Boville, B. A., Sassi, F., Solomon, S. C., and Matthes, K.: Modeling the whole atmosphere response to solar cycle changes in radiative and geomagnetic forcing, *Journal of Geophysical Research: Atmospheres*, 112, <https://doi.org/https://doi.org/10.1029/2006JD008306>, 2007.
- Mekhaldi, F., Muscheler, R., Adolphi, F., Aldahan, A., Beer, J., McConnell, J., Possnert, G., Sigl, M., Svensson, A., Synal, H.-A., Welten, K., and Woodruff, T.: Multiradionuclide evidence for the solar origin of the cosmic-ray events of AD 774/5 and 993/4, *Nature communications*, 6, 8611, <https://doi.org/10.1038/ncomms9611>, 2015.
- 880 Meraner, K. and Schmidt, H.: Climate impact of idealized winter polar mesospheric and stratospheric ozone losses as caused by energetic particle precipitation, *Atmospheric Chemistry and Physics*, 18, 1079–1089, <https://doi.org/10.5194/acp-18-1079-2018>, 2018.
- Meyer, P., Parker, E. N., and Simpson, J. A.: Solar Cosmic Rays of February, 1956 and Their Propagation through Interplanetary Space, *Phys. Rev.*, 104, 768–783, <https://doi.org/10.1103/PhysRev.104.768>, 1956.
- 885

- Nieder, H., Winkler, H., Marsh, D., and Sinnhuber, M.: NO<sub>x</sub> production due to energetic particle precipitation in the MLT region: Results from ion chemistry model studies, 119, 2014.
- Porter, H. S., Jackman, C. H., and Green, A. E. S.: Efficiencies for production of atomic nitrogen and oxygen by relativistic proton impact in air, *The Journal of Chemical Physics*, 65, 154–167, <https://doi.org/10.1063/1.432812>, 1976.
- 890 Rodger, C. J., Verronen, P. T., Clilverd, M. A., Seppälä, A., and Turunen, E.: Atmospheric impact of the Carrington event solar protons, *Journal of Geophysical Research: Atmospheres*, 113, <https://doi.org/https://doi.org/10.1029/2008JD010702>, 2008.
- Rohen, G., von Savigny, C., Sinnhuber, M., Llewellyn, E. J., Kaiser, J. W., Jackman, C. H., Kallenrode, M.-B., Schröter, J., Eichmann, K.-U., Bovensmann, H., and Burrows, J. P.: Ozone depletion during the solar proton events of October/November 2003 as seen by SCIAMACHY, *Journal of Geophysical Research: Space Physics*, 110, <https://doi.org/https://doi.org/10.1029/2004JA010984>, 2005.
- 895 Rusch, D., Gérard, J.-C., Solomon, S., Crutzen, P., and Reid, G.: The effect of particle precipitation events on the neutral and ion chemistry of the middle atmosphere—I. Odd nitrogen, *Planetary and Space Science*, 29, 767–774, [https://doi.org/https://doi.org/10.1016/0032-0633\(81\)90048-9](https://doi.org/https://doi.org/10.1016/0032-0633(81)90048-9), 1981.
- Sander, S., Golden, D., Kurylo, M., Moortgat, G., Wine, P., Ravishankara, A., Kolb, C., Molina, M., Finlayson-Pitts, B., Huie, R., et al.: Chemical kinetics and photochemical data for use in atmospheric studies evaluation number 15, Tech. rep., Pasadena, CA: Jet Propulsion Laboratory, National Aeronautics and Space . . . , 2006.
- 900 Sinnhuber, M., Nieder, H., and Wieters, N.: Energetic Particle Precipitation and the Chemistry of the Mesosphere/Lower Thermosphere, *Surveys in Geophysics*, 33, <https://doi.org/10.1007/s10712-012-9201-3>, 2012.
- Solomon, S., Rusch, D., Gérard, J., Reid, G., and Crutzen, P.: The effect of particle precipitation events on the neutral and ion chemistry of the middle atmosphere: II. Odd hydrogen, *Planetary and Space Science*, 29, 885–893, [https://doi.org/https://doi.org/10.1016/0032-0633\(81\)90078-7](https://doi.org/https://doi.org/10.1016/0032-0633(81)90078-7), 1981.
- 905 Stiller, G. P., Kiefer, M., Eckert, E., von Clarmann, T., Kellmann, S., García-Comas, M., Funke, B., Leblanc, T., Fetzer, E., Froidevaux, L., Gomez, M., Hall, E., Hurst, D., Jordan, A., Kämpfer, N., Lambert, A., McDermid, I. S., McGee, T., Miloshevich, L., Nedoluha, G., Read, W., Schneider, M., Schwartz, M., Straub, C., Toon, G., Twigg, L. W., Walker, K., and Whiteman, D. N.: Validation of MIPAS IMK/IAA temperature, water vapor, and ozone profiles with MOHAVE-2009 campaign measurements, *Atmospheric Measurement Techniques*, 5, 289–320, <https://doi.org/10.5194/amt-5-289-2012>, 2012.
- 910 Sukhodolov, T., Usoskin, I. G., Rozanov, E. V., Asvestari, E., Ball, W. T., Curran, M. A. J., Fischer, H., Kovaltsov, G. A., Miyake, F., Peter, T., Plummer, C., Schmutz, W. K., Severi, M., and Traversi, R.: Atmospheric impacts of the strongest known solar particle storm of 775 AD, *Scientific Reports*, 7, 2017.
- Swider, W. and Keneshea, T.: Decrease of ozone and atomic oxygen in the lower mesosphere during a PCA event, *Planetary and Space Science*, 21, 1969–1973, [https://doi.org/https://doi.org/10.1016/0032-0633\(73\)90126-8](https://doi.org/https://doi.org/10.1016/0032-0633(73)90126-8), 1973.
- 915 Turco, R. P.: On the formation and destruction of chlorine negative ions in the D region, *Journal of Geophysical Research (1896-1977)*, 82, 3585–3592, <https://doi.org/https://doi.org/10.1029/JA082i025p03585>, 1977.
- Usoskin, I. G. and Kovaltsov, G. A.: OCCURRENCE OF EXTREME SOLAR PARTICLE EVENTS: ASSESSMENT FROM HISTORICAL PROXY DATA, *The Astrophysical Journal*, 757, 92, <https://doi.org/10.1088/0004-637x/757/1/92>, 2012.
- 920 Usoskin, I. G., Kromer, B., Ludlow, F., Beer, J., Friedrich, M., Kovaltsov, G. A., Solanki, S. K., and Wacker, L.: The AD775 cosmic event revisited: the Sun is to blame, *Astronomy and Astrophysics*, 552, 2013.
- Verronen, P., Seppälä, A., Clilverd, M., Rodger, C., Kyrölä, E., Enell, C.-F., Ulich, T., and Turunen, E.: Diurnal variation of ozone depletion during the October–November 2003 solar proton events, *J. Geophys. Res.*, 110, <https://doi.org/10.1029/2004JA010932>, 2005.

- Verronen, P. T., Andersson, M. E., Marsh, D. R., Kovács, T., and Plane, J. M. C.: WACCM-D—Whole Atmosphere  
925 Community Climate Model with D-region ion chemistry, *Journal of Advances in Modeling Earth Systems*, 8, 954–975,  
<https://doi.org/https://doi.org/10.1002/2015MS000592>, 2016.
- von Clarmann, T., Glatthor, N., Höpfner, M., Kellmann, S., Ruhnke, R., Stiller, G. P., Fischer, H., Funke, B., Gil-López, S., and López-  
Puertas, M.: Experimental evidence of perturbed odd hydrogen and chlorine chemistry after the October 2003 solar proton events, *Journal*  
*of Geophysical Research: Space Physics*, 110, <https://doi.org/https://doi.org/10.1029/2005JA011053>, 2005.
- 930 von Clarmann, T., Glatthor, N., Grabowski, U., Höpfner, M., Kellmann, S., Linden, A., Mengistu Tsidu, G., Milz, M., Steck, T., Stiller,  
G. P., Fischer, H., and Funke, B.: Global stratospheric HOCl distributions retrieved from infrared limb emission spectra recorded  
by the Michelson Interferometer for Passive Atmospheric Sounding (MIPAS), *Journal of Geophysical Research: Atmospheres*, 111,  
<https://doi.org/https://doi.org/10.1029/2005JD005939>, 2006.
- von Clarmann, T., Funke, B., Glatthor, N., Kellmann, S., Kiefer, M., Kirner, O., Sinnhuber, B.-M., and Stiller, G. P.: The MIPAS HOCl  
935 climatology, *Atmospheric Chemistry and Physics*, 12, 1965–1977, <https://doi.org/10.5194/acp-12-1965-2012>, 2012.
- von Clarmann, T., Degenstein, D. A., Livesey, N. J., Bender, S., Braverman, A., Butz, A., Compernelle, S., Damadeo, R., Dueck, S., Eriksson,  
P., Funke, B., Johnson, M. C., Kasai, Y., Keppens, A., Kleinert, A., Kramarova, N. A., Laeng, A., Langerock, B., Payne, V. H., Rozanov,  
A., Sato, T. O., Schneider, M., Sheese, P., Sofieva, V., Stiller, G. P., von Savigny, C., and Zawada, D.: Overview: Estimating and report-  
ing uncertainties in remotely sensed atmospheric composition and temperature, *Atmospheric Measurement Techniques*, 13, 4393–4436,  
940 <https://doi.org/10.5194/amt-13-4393-2020>, 2020.
- Weeks, L. H., Cuikay, R. S., and Corbin, J. R.: Ozone Measurements in the Mesosphere During The Solar Proton Event of 2 November 1969,  
*Journal of Atmospheric Sciences*, 29, 1138 – 1142, [https://doi.org/10.1175/1520-0469\(1972\)029<1138:OMITMD>2.0.CO;2](https://doi.org/10.1175/1520-0469(1972)029<1138:OMITMD>2.0.CO;2), 1972.
- Winkler, H., Kazeminejad, S., Sinnhuber, M., Kallenrode, M.-B., and Notholt, J.: Conversion of mesospheric HCl into active chlo-  
rine during the solar proton event in July 2000 in the northern polar region, *Journal of Geophysical Research: Atmospheres*, 114,  
945 <https://doi.org/https://doi.org/10.1029/2008JD011587>, 2009.
- Winkler, H., Kazeminejad, S., Sinnhuber, M., Kallenrode, M.-B., and Notholt, J.: Correction to “Conversion of mesospheric HCl into active  
chlorine during the solar proton event in July 2000 in the northern polar region”, *Journal of Geophysical Research: Atmospheres*, 116,  
<https://doi.org/https://doi.org/10.1029/2011JD016274>, 2011.
- Wissing, J. M. and Kallenrode, M.-B.: Atmospheric Ionization Module Osnabrück (AIMOS): A 3-D model to determine atmo-  
950 spheric ionization by energetic charged particles from different populations, *Journal of Geophysical Research: Space Physics*, 114,  
<https://doi.org/https://doi.org/10.1029/2008JA013884>, 2009.